2017

Gravitational Microlensing

Wesley M. Barnes
Virginia Commonwealth University

Gravitational Microlensing

by

Wesley Michael Barnes

A thesis presented to the Department of Physics

in partial fulfillment of the requirements for the degree of

Master of Science

in the subject of Physics

Virginia Commonwealth University

Richmond, Virginia

May, 2017

Abstract

A gravitational microlensing event occurs when a foreground star passes near our line of site to a background source star. The foreground star acts as a lens, perturbing the image of the source star and amplifying the apparent intensity. Because the lens is in motion relative to the source star, the amplification is a function in time, resulting in a characteristic microlensing light curve. If the lens happens to have a planetary companion, the resulting light curve will be perturbed due the planet and the characteristics of the binary system can be ascertained.

Acknowledgments

I would like to thank Dr. Robert Gowdy for taking the time to teach me general relativity and for his help in completing this work. I thank Dr. Marilyn Bishop for her guidance with Mathematica. I thank Amanda Steck for her support during these past two years. Lastly, I thank my parents, Kevin and Denise Barnes for their encouragement and support throughout my academic career.

Contents

List of Figures

Introduction

Gravitational lensing was first proposed by Albert Einstein during the preparation of his theory of general relativity. He noted that because massive objects curve spacetime, the path of light passing near those massive objects will bend light around them. In fact, it was gravitational lensing that made Einstein a household name as the deflection of light around the sun was used to test his theory during a solar eclipse. Since that time, gravitational lensing has become an indispensable tool for astronomers. This thesis focuses on a special class of gravitational lensing known as microlensing and examines some of the techniques used.

The field of gravitational lensing can be broken down into three basic regimes: strong lensing, weak lensing, and microlensing.[26] Strong lensing is characterized by a lens creating very substantial image distortions culminating in multiple images, large luminous arcs, and occasionally Einstein rings. These image distortions can be seen through telescopes. Figure 1 shows a particularly clear example of a large arc nearly forming an Einstein ring taken by the Hubble Telescope.

Weak lensing is characterized by small deviations in the image of background galaxies and galaxy clusters. The lensed images of background sources are still resolvable, however statistical analysis is necessary to determine if gravitational lensing is taking place. This is because the images are not distorted enough to differentiate between gravitational lensing and the regular orientation of a galaxy.

The final regime, microlensing, is characterized by very small deviations in the path of

Figure 1: A Hubble image of a gravitational lens. A foreground galaxy lenses a background galaxy resulting in a large luminous arc around the lens.

light rays. The images formed are similar to that of strong lensing, but are too small to resolve with current generation of telescopes. This doesn't exclude microlensing from being incredibly useful. The microlensing effects that can be measured, namely the amplification of a source star's brightness, is used to determine information about the lens such as mass and distance from the earth. While strong and weak lensing focus primarily on the images formed by gravitational lensing, microlensing focuses exclusively on the amplification of the background source.

Gravitational lensing due to the close alignment of a foreground lens and a background source star, what we now call microlensing, was first published by Einstein in 1936.[8] However, he dismissed the practicality of microlensing, stating that "there is no great chance of observing this phenomenon." Of course, he is correct in that the probability of close alignment of two stars within our galaxy is on the order of 10^{-6}. Thus, the field of gravitational microlensing lay dormant until the publication of Paczynski's paper on the subject.[23] Paczynski recognized that the advent of CCDs and the high speed computing required to analyze their images made it possible to observe a large number of stars simultaneously. He concluded that such a survey would make it possible, and likely, that microlensing could indeed be observed in modern times.

Microlensing was first used to search for Massive Compact Halo Objects (MACHO), which are dark stars in the outer ring of our galaxy.[2] At the time, MACHOs were thought

to be a significant contribution to dark matter within our galaxy. Large scale surveys were conducted and thousands of microlensing events have since been observed, although the idea that MACHOs contribute to dark matter has largely been discredited.

Even before the first microlensing events were observed, Mao and Paczynski suggested that microlensing could be used to exoplanets orbiting around lens.[20] A planet has a characteristic effect on the overall amplification of a source star and thus could be detected using similar techniques to that of the MACHO search. Gould and Loeb considered this and developed a "two tier" procedure for detecting planetary microlensing events.[16] First, a single survey monitors a large number of stars in the galactic bulge, searching for the signature amplification due to the primary lens. Second, an alert is put out to a large number of observatories to monitor the event continuously for many days. Since the implementation of this procedure, 44 planets have been detected by microlensing.

Chapter 1 introduces the necessary principles of general relativity required to derive the deflection angle of light around a star, beginning with the basic mathematical constructs of differential geometry and their applications to general relativity. The geodesic equation is introduced to describe the path of a light ray in curved spacetime. The Schwarzschild metric is then used to calculate the deflection angle of a light ray.

Chapter 2 introduces the basic geometry of a single lens microlensing event. The single lens microlensing event is used as the building block to more complicated models discussed in later chapters. Common nomenclature present in modern microlensing literature is introduced, as well as the degeneracy present in the basic model.

Chapter 3 introduces two new measurable quantities by relaxing the assumptions made in the single lens case described in Chapter 2, namely, the angular Einstein radius and the projected Einstein radius. Techniques for measuring the angular Einstein radius, and the projected Einstein radius are discussed leading to a complete solution to a microlensing event.

Chapter 4 discusses the application of microlensing to discovering exoplanets. The lens

equation and amplification due to a single lens is generalized to N bodies. A detailed description of a binary lens is discussed, introducing the additional structure called critical and caustic curves. A detailed discussion of caustic curves in planetary events are described as well as their effect on the light curve of an event.

Chapter 1

Deflection angle of light

This chapter will focus on deriving the deflection angle of a light ray passing near a massive object. This requires the use of General Relativity. As such, most of this chapter will be devoted to defining some of the fundamental concepts of differential geometry. We start with a basic explanation of differential geometry which deals with smoothly curved surfaces (manifolds).

1.1 Manifolds

Much of physics revolves around the vector space $\mathbb{R}^3$, or more generally, $\mathbb{R}^n$. Flat space is intuitive and easy to work with. We understand how to differentiate and integrate in $\mathbb{R}^n$, among other things. General Relativity requires the use of other more generalized spaces known as manifolds, of which $\mathbb{R}^n$ is the simplest example. Simply put, a manifold is a smoothly curved space (the surface of sphere for example), but locally it "looks like" $\mathbb{R}^n$. We describe a manifold by smoothly overlapping these locally flat regions together.[5]

To be a little more precise, a manifold is a set M. We map a subset $U \subset M$ into $\mathbb{R}^n$ where we can assign coordinates to the points in U. In this way, we can cover M with multiple overlapping coordinate maps called charts to describe the entire manifold. The collection of coordinate charts is referred to as an atlas.

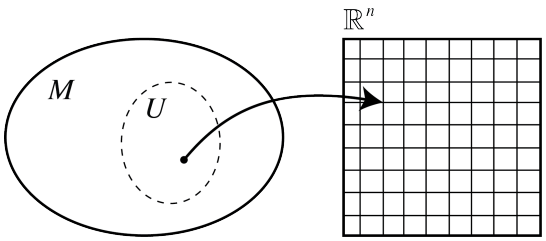

Figure 1.1: A point in the subset $U \subset M$ is mapped to a point in $\mathbb{R}^n$.

1.2 Tangent space

Now that we have an idea of what a manifold is, we need to introduce the concept of a tangent space. The tangent space, T_p, is a vector space associated with a single point, P, in the manifold M. The vectors in tangent space are directional derivatives tangent to a curve, f, parameterized by λ, at the point P. Thus we can write a vector in the tangent space, $v \in T_P$, as,

$$v = \left(\frac{\partial f}{\partial \lambda}\right) = \sum_i^n \left(\frac{dx^i}{d\lambda}\frac{\partial}{\partial x^i}\right) f = \sum_i^n \left(v^i e_i\right) f \tag{1.1}$$

where $v^i = dx^i/d\lambda$ and $e_i = \partial/\partial x^i$. The basis vectors e_i are known as the coordinate basis. The vector, v, can be written as,

$$v = \sum_i^n \left(v^i e_i\right) \tag{1.2}$$

with the understanding that v is the tangent vector to a curve f on the manifold. We can introduce a new notation to make writting out vectors easier. The compenents of a vector have an upper index and the basis vectors have a lower index. Whenever an upper and lower index is repeated, the summation over that index is implied. This is known as the Einstein summation convention. Using this convention, we can write the vector v as,

$$v = \sum_i^n v^i e_i = v^i e_i \text{ (Enstein summation convention)} \tag{1.3}$$

1.3 Metric tensor

The metric tensor, g, is an important concept in General Relativity. It allows us to compute the scalar product of two vectors v and u by,[5]

$$g(v, u) = v \cdot u \tag{1.4}$$

We can expand the vectors v and u using their basis to get,

$$g(v, u) = g(v^i e_i, u^j e_j) = g(e^i, e^j) v^i u^j = g_{ij} v^i u^j \tag{1.5}$$

where g_{ij} are the scalar products of the basis vectors, also called the coefficients of the metric tensor. In four-dimensional spacetime, the metric tensor can be reresented as a 4×4 matrix,

$$g_{ij} = \begin{pmatrix} g_{00} & g_{01} & g_{02} & g_{03} \\ g_{10} & g_{11} & g_{12} & g_{13} \\ g_{20} & g_{21} & g_{22} & g_{23} \\ g_{30} & g_{31} & g_{32} & g_{33} \end{pmatrix} \tag{1.6}$$

The metric tensor can be used to define the line element ds in space-time. If we insert the infinitesimal change in position vector into the metric tensor, we get,

$$ds^2 = g(du, du) = g(du^i e_i, du^j e_j) = g_{ij} du^i du^j \tag{1.7}$$

A particularly important example of a line element in Minkowski space-time, the analog of flat Euclidean space in special relativity. The metric tensor in minkowski space-time is given

as,

$$g_{ij} = \begin{pmatrix} -c^2 & 0 & 0 & 0 \\ 0 & 1 & 0 & 0 \\ 0 & 0 & 1 & 0 \\ 0 & 0 & 0 & 1 \end{pmatrix} \tag{1.8}$$

and thus the line element is,

$$ds^2 = -c^2dt^2 + dx^2 + dy^2 + dz^2 \tag{1.9}$$

where c is the speed of light and dt is an infinitesimal change in time between two events. We classify the line elements by their signature, i.e by the signs of the terms in the line element. In this thesis, we will use the signature $(-,+,+,+)$, although we can also write Equation 1.9 using the signature $(+,-,-,-)$ which is common in quantum field theory. The signature distinguishes between space-like intervals, for which $ds^2 > 0$, time-like intervals, for which $ds^2 < 0$, and light-like intervals, for which $ds^2 = 0$. We will be interested in light-like intervals in deriving the deflection angle of light.

1.4 Covarient derivative

Consider the derivative of a vector v with respect to a parameter λ. By expanding the vector in terms of its basis vectors, we can write the derivative as,[5]

$$\frac{dv}{d\lambda} = \frac{d}{d\lambda}(v^i e_i) = \frac{dv^i}{d\lambda}e_i + v^i\frac{de_i}{d\lambda} = \frac{\partial v^i}{\partial x^j}v^j e_i + v^i\frac{\partial e_i}{\partial x^j}v^j \tag{1.10}$$

In Cartesian coordinates, $\frac{\partial e_i}{\partial x^j} = 0$ since the basis vectors are constant. However, when we have curved coordinates, the basis vectors will change. Introducing a new symbol, the connection coefficients Γ^j,

$$\frac{\partial e_i}{\partial x^j} = \Gamma^k_{ij}e_k \tag{1.11}$$

tells us how the basis vectors change over the manifold. Then we can write Equation 1.10 as,

$$\frac{dv}{d\lambda} = \frac{\partial v^i}{\partial x^j}\frac{\partial x^j}{\partial \lambda}e_i + \Gamma^k_{ij}v^i\frac{\partial x^j}{\partial \lambda}e_k \tag{1.12}$$

Changing the indices in the second term ($i \to k$ and $k \to i$), we can write this as, [5]

$$\frac{dv}{d\lambda} = \left(\frac{\partial v^i}{\partial x^j}\frac{\partial x^j}{\partial \lambda} + \Gamma^i_{kj}v^k\frac{\partial x^j}{\partial \lambda}\right)e_i \tag{1.13}$$

The connection coefficients can be found by using the metric tensor and its inverse,[5]

$$\Gamma^i_{kj} = \frac{1}{2}g^{i\ell}\left(\frac{\partial g_{j\ell}}{\partial x^k} + \frac{\partial g_{k\ell}}{\partial x^i} - \frac{\partial g_{kj}}{\partial x^\ell}\right) \tag{1.14}$$

Equation 1.13 defines the covarient derivative, denoted $D_u v$, as the derivative of the vector v is taken in the direction of the vector u.[5]

$$D_u v = \left(\frac{\partial v^i}{\partial x^j}\frac{\partial x^j}{\partial \lambda} + \Gamma^i_{kj}v^k\frac{\partial x^j}{\partial \lambda}\right)e_i \tag{1.15}$$

If we take the covarient derivative in the direction of v, namely $D_v v$, we get,

$$D_v v = 0 \tag{1.16}$$

This is known as the geodesic equation. It is the generalization of a "straight line" in curved spacetime, thus it gives the path of a light ray (or free falling particle). In terms of the components, the geodesic equation reads,

$$\frac{\partial v^i}{\partial x^j}\frac{\partial x^j}{\partial \lambda} + \Gamma^i_{kj}v^k\frac{\partial x^j}{\partial \lambda} = 0 \tag{1.17}$$

or equivalently,

$$\frac{d^2x^i}{d\lambda^2} + \Gamma^i_{kj}\frac{\partial x^k}{\partial \lambda}\frac{\partial x^j}{\partial \lambda} = 0 \tag{1.18}$$

The fact that $D_v v = 0$ constrains the parameter λ to be an affine parameter. In other words, as you translate the vector v along the manifold, so long as you keep the vector parallel and of the same magnitude, you define the path along the manifold and in doing so, define the parameter of the path. For a time-like curve, (i.e. massive particles) the parameter λ is the proper time, τ. For light-like paths, the proper time does not work because $\tau = 0$. However, if we find a path such that a curve parametarized by λ such that $D_v v = 0$ is true, then any parameter of the form $a\lambda + b$ is also an affine parameter. Thus, there is no preferred parameter for light-like curves. We are free to choose any parameter so long as the curve follows $D_v v = 0$.

1.5 Schwarzschild metric

The metric is found for a particular spacetime by solving Einstein's field equations. Because we are interested in the spacetime outside of a star, Einstien's field equations take the simple form,[5]

$$R_{\mu\nu} = 0 \tag{1.19}$$

These equations are called the Vacuum field equations and $R_{\mu\nu}$ is the Ricci tensor. The Ricci tensor is related to what is called the curvature tensor by,[5]

$$R_{\mu\nu} = R^{\lambda}_{\mu\lambda\nu} \tag{1.20}$$

The curvature tensor is a four dimensional tensor which describes the curvature at a point in spacetime. We find the curvature tensor from the connection coefficients by,[5]

$$R^{\lambda}_{\mu\rho\nu} = \frac{\partial}{\partial_\rho}\Gamma^{\lambda}_{\nu\mu} - \frac{\partial}{\partial_\nu}\Gamma^{\lambda}_{\rho\mu} + \Gamma^{\lambda}_{\rho\sigma}\Gamma^{\sigma}_{\nu\mu} - \Gamma^{\lambda}_{\nu\sigma}\Gamma^{\sigma}_{\rho\mu} \tag{1.21}$$

Because stars are spherically symmetric, we want the spacetime which solves Equation 1.19 to be spherically symmetric as well. For the moment, consider the Minkowski metric in

spherical coordinates,[5]

$$ds^2_{flat} = -cdt^2 + dr^2 + r^2(d\theta^2 + \sin^2\theta d\phi^2) \tag{1.22}$$

A general metric which preserves spherical symmetry is a metric of the form,[5]

$$ds^2 = -A(r)cdt^2 + B(r)dr^2 + C(r)r^2(d\theta^2 + \sin^2\theta d\phi^2) \tag{1.23}$$

where $A(r)$, $B(r)$, and $C(r)$ are arbitrary functions of the radial coordinate r and preserve the metric signature $(-,+,+,+)$. To find the functions $A(r)$, $B(r)$, and $C(r)$, we solve Einstien's field equations by first finding the connection coefficients using Equation 1.14, then calculating the curvature tensor using Equation 1.21, and finally, finding the Ricci tensor using Equation 1.20. This requires a lot of work and calculation, but the solution you get is known as the Schwarzschild metric, given by,[5]

$$ds^2 = -\left(1 - \frac{R_S}{r}\right)c^2dt^2 + \left(1 - \frac{R_S}{r}\right)^{-1}dr^2 + r^2(\sin^2\theta d\phi^2 + d\theta^2) \tag{1.24}$$

which describes the spacetime outside of spherically symmetric, non-rotating masses, where $R_S = 2Gm/c^2$. The Schwarzschild metric is an excellent approximation for describing the spacetime outside of stars and planets which will be useful for deriving the deflection angle of light. Here we will discuss some of the properties of the Schwarzschild geometry.

When $r = R_S$, we see that the second term in Equation 1.24 diverges. This is a coordinate singularity which can be resolved by changing the coordinates. R_S is known as the Schwarzschild radius which is where the event horizon for a black hole is formed. If we let $r \to \infty$, the metric reduces to flat Minkowski spacetime. Because the outside radius of a planet or star is much greater than the Schwarzschild radius, spacetime can be considered essentially flat with a small perturbation from Minkowski space. We will take advantage of this later.

Due to the spherical symmetry of the Schwarzschild metric, the path of a free falling particle will not depend on the angle θ. This means we are free to choose any value of θ. If we choose $\theta = \pi/2$, the metric reduces to,

$$ds^2 = -\left(1 - \frac{R_S}{r}\right) c^2 dt^2 + \left(1 - \frac{R_S}{r}\right)^{-1} dr^2 + r^2 d\phi^2 \tag{1.25}$$

This is the form we will use to derive the deflection angle of light.

Using Equation 1.14, we find the connection coefficients for the Schwarzschild metric. Using the labels (t, r, θ, ϕ) in place of (0,1,2,3), we find the non-zero connection coefficients to be,

$$\Gamma^r_{rr} = \frac{1}{2}\frac{R_S}{r^3}(r - R_S) \qquad \Gamma^t_{tr} = -\Gamma^r_{tt} = \frac{R_S}{2r(r - R_S)}$$

$$\Gamma^\theta_{r\theta} = \Gamma^\phi_{r\phi} = \frac{1}{r} \qquad \Gamma^r_{\theta\theta} = \Gamma^r_{\phi\phi} = -(r - R_S)$$

1.6 Deflection Angle of light around a star or planet

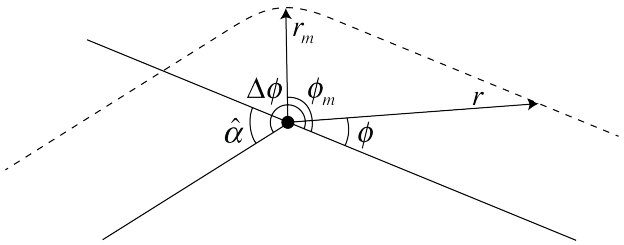

Figure 1.2: The geometry of a light ray passing near a spherically symmetric mass. $\Delta\phi$ is the total change in the angle ϕ, $\hat{\alpha}$ is the change in angle of the path of the light ray, and r_m is the point of closest approach of the light ray to the mass, called the impact parameter.

In order to derive the deflection angle of light around a star or planet, we first need to solve the geodesic equation given in Equation 1.18. The geodesic equation gives the four second-order differential equations. We will only need two of them in order to find the

deflection angle. The geodesic for the t coordinate is given by,

$$\ddot{t} + \frac{R_S}{r(r - R_S)}\dot{r}\dot{t} = 0 \quad \rightarrow \quad \frac{d}{d\lambda}\left[\left(1 - \frac{R_S}{r}\right)\dot{t}\right] = 0 \tag{1.26}$$

and the geodesic equation for ϕ is given by,

$$\ddot{\phi} + \frac{2}{r}\dot{\phi}\dot{r} = 0 \quad \rightarrow \quad \frac{d}{d\lambda}\left(r^2\dot{\phi}\right) = 0 \tag{1.27}$$

The terms inside of the brackets in Equations 1.26 and 1.27 must be equal to constant values, thus we can write,

$$\left(1 - \frac{R_S}{r}\right)\dot{t} = a \text{ (constant)} \tag{1.28}$$

$$r^2\dot{\phi} = b \text{ (constant)} \tag{1.29}$$

We have an additional constraint that $ds^2 = 0$ for light rays, thus from Equation 1.25 we have

$$-\left(1 - \frac{R_S}{r}\right)c^2dt^2 + \left(1 - \frac{R_S}{r}\right)^{-1}dr^2 + r^2d\phi^2 = 0 \tag{1.30}$$

Combining Equations 1.28, 1.29, and 1.30, along with scaling the parameter λ such that $a = c^2$, we have

$$\dot{r}^2 = 1 - \frac{b^2}{r^2}\left(1 - \frac{R_S}{r}\right) \tag{1.31}$$

What we are looking for is a way to relate the change in ϕ as a function of r. We do this by combining the result from Equation 1.31 with Equation 1.29 to get

$$d\phi = \frac{b}{r^2}\left[1 - \frac{b^2}{r^2}\left(1 - \frac{R_S}{r}\right)\right]^{-1/2}dr \tag{1.32}$$

We can now find the total deflection angle by integration. As shown in Figure 1.2, if a light

ray comes from $r = \infty$, the total change in ϕ, $\Delta\phi$, is given by,

$$\Delta\phi = 2\int_{\infty}^{r_m} \frac{b}{r^2}\left[1 - \frac{b^2}{r^2}\left(1 - \frac{R_S}{r}\right)\right]^{-1/2} dr \tag{1.33}$$

where r_m is the point of closest approach of the light ray to the star, typically called the impact parameter. The impact parameter results in an inflection point along the path of the light ray where,

$$\frac{dr}{d\phi} = \frac{b}{r^2}\left[1 - \frac{b^2}{r^2}\left(1 - \frac{R_S}{r}\right)\right]^{-1/2} = 0 \tag{1.34}$$

This relation allows us to solve for the constant b:

$$b = r_m\left(1 - \frac{R_S}{r_m}\right)^{-1/2} \tag{1.35}$$

Combining with Equation 1.33 and making the substitution $u = r_m/r$ gives the total change in ϕ as,

$$\Delta\phi = 2\int_0^1 \left[1 - u^2 - \frac{R_S}{r_m}(1 - u^3)\right]^{-1/2} du \tag{1.36}$$

The minimum value r_m can take on is the radius of the star or planet. Thus, $r_m \gg R_S$. We can expand the integrand in Equation 1.36 for small values of R_S/r_m, keeping only the linear terms to give,

$$\Delta\phi = 2\int_0^1 \left[\frac{1}{\sqrt{1-u^2}} - \frac{R_S}{2r_m}\frac{(u^3-1)}{(1-u^2)^{3/2}}\right] du = \pi + \frac{2R_S}{r_m} \tag{1.37}$$

From the geometry is Figure 1.2, we can define the deflection angle $\hat{\alpha}$ to be,

$$\hat{\alpha} = \Delta\phi - \pi = \frac{2R_S}{r_m} \tag{1.38}$$

We arrive at the final form for the deflection angle by recalling that $R_S = 2Gm/c^2$,

$$\hat{\alpha} = \frac{4Gm}{c^2 r_m} \tag{1.39}$$

Because we made the approximation that $r_m \gg R_S$, the deflection angle is only valid for small angles. This is a good approximation for the deflection angle outside of stars and planets.

Chapter 2

Basic Microlensing

In chapter one, we derived the deflection angle of a light ray passing near a spherically symmetric massive object. Microlensing concerns itself with the light rays deflected by a massive object that reach an observer (either a satellite or an observatory on Earth). In this chapter, we define the microlensing geometry and explore how the source appears from the observer's perspective. In the process, we also define the assumptions, vocabulary, and observable parameters of microlensing events.

2.1 Geometry of a Lensing Event

Figure 2.1 depicts the geometry of a lensing event.[26] Consider a source star, S, a distance D_S from an observer. We define the source sphere, S_S, as the sphere of radius D_S centered about the observer. The source star lies on the surface of the sphere. A spherically symmetric lens, L, lies in between the source star and the observer at a distance D_L away from the observer. We define a second sphere, the lens sphere S_L, as sphere of radius D_L centered on the observer with the lens on the surface of the sphere. We define a third sphere, the observer's sphere S_O, as a sphere a small distance away from the observer compared with D_L that sphere acts as the sky the observer sees. A line can be extended from the observer through the position of the lens that intersects the source sphere at a point N. This is called

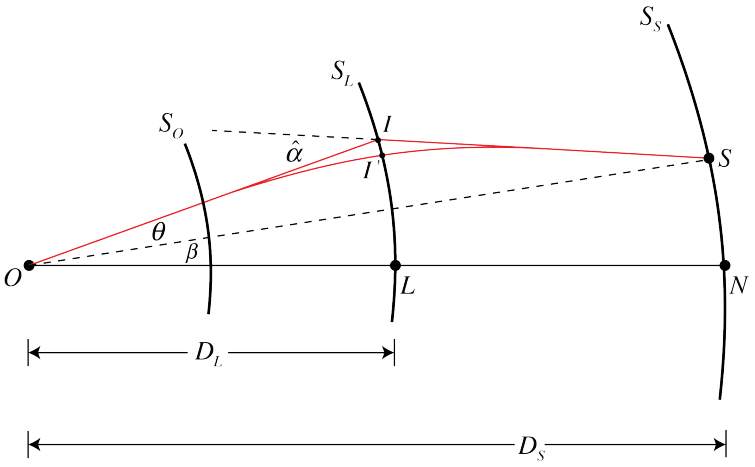

Figure 2.1: The geometry of a microlensing event. The source star, assumed to be a point source, lies in the source sphere S_S of radius D_S while a lens, assumed to be a point lens, lies in the lens sphere S_L of radius D_L. The observer's sky is the sphere S_O. The red line depicts the path of a light ray originating from the source star as it passes near the lens, deflected by an angle $\hat{\alpha}$. The point I' is the position of the image the observer sees at an angle θ with respect to the optic axis. The angle β is the angular lens-source separation.

the optic axis and is used as a reference.

A light ray emanating from the source star passing near the lens is deflected through a point I on the lens sphere. Asymptotes are drawn from the source star and the observer, intersecting at a point I' on the lens plane. The angle $\hat{\alpha}$ is the total angle of deflection of the light ray as defined in Chapter 1. The dotted line drawn from the observer to the source is the path a light ray would take to reach the observer were it not for the lens. This serves to define the angle β, the angular position of the source with respect to the optic axis. The angle β is known as the angular lens-source separation as seen from the observer's sphere. The angle θ is the angle of the incoming light ray with respect to the point I, known as the image position in the observer's plane.

Observed microlensing events take place within our galaxy.[23] This means the radius of the lens sphere and source sphere, D_L and D_S, are very large. Because $\hat{\alpha}$ is small, θ and β are also small. Thus, using a small angle approximation, the three spheres defined above are essentially flat in the region of interest. We can replace the spheres with planes, as depicted in Figure 2.2. In addition, the difference between the points I and I' in Figure

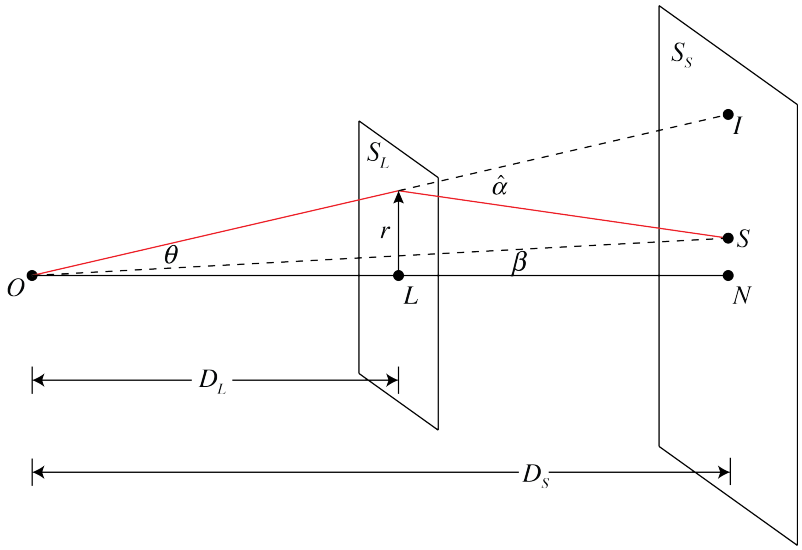

Figure 2.2: The geometry of the thin lens approximation used in microlensing events. A source star lies in the source plane S_S and a lens lies in the plane S_L. The red line is the path of a light ray originating from a source star a distance D_S from an observer O. The deflection angle $\hat{\alpha}$ is due to the lens L a distance D_L from the observer. The light passes the lens with an impact parameter r. The angle θ is the position of an image of the source star as seen from the observer. The angle β is the lens-source separation.

2.1 is negligible, i.e., $I \approx I'$.[26] This allows us to consider all of the deflection taking place within the lens plane, S_L. This is known as the "thin lens approximation" and is analogous to the thin lens approximation in optics. Figure 2.2 also shows the impact parameter r. The observer plane, S_O, is redefined as the plane in which the observer lies. All of the planes are perpendicular to the optic axis.

2.2 Lens Equation for a Single Lens

Our goal now is to relate the observed image positions of the source with respect to the actual source position in the presence of a point lens. This is known as the "lens equation."[26] From the geometry in Figure 2.2, we can write

$$\beta D_S = \theta D_S - \hat{\alpha}(D_S - D_L) \tag{2.1}$$

The impact parameter $r_m = D_L\theta$, thus we can write $\hat{\alpha}$ from Equation 1.39 in terms of θ as,

$$\hat{\alpha} = \frac{4Gm}{c^2 D_L \theta} \tag{2.2}$$

Inserting Equation 2.2 this into 2.1 and dividing both sides by D_S gives,

$$\beta = \theta - \frac{4GM}{c^2\theta}\frac{D_S - D_L}{D_S D_L} \tag{2.3}$$

Defining a new variable, the reduced deflection angle,

$$\alpha(\theta) = \frac{4GM}{c^2\theta}\frac{D_S - D_L}{D_S D_L} = \hat{\alpha}\frac{(D_S - D_L)}{D_L} \tag{2.4}$$

we can rewrite Equation 2.3 in a simple form,[26][21][25]

$$\beta = \theta - \alpha(\theta) \tag{2.5}$$

The lens equation can be thought of as a mapping from the angular position of the source in the source plane to the angular positions of the images in the lens plane. This mapping is not in general one-to-one as we will see below.

2.3 Einstein Ring

A special case occurs when the observer, lens, and source align. The lens-source separation $\beta = 0$ and Equation 2.3 can be written as,

$$\theta = \alpha = \frac{(D_S - D_L)}{D_S D_L}\frac{4Gm}{c^2\theta} \tag{2.6}$$

Solving for the image position, θ, gives a special quantity,

$$\theta = \theta_E \equiv \sqrt{\frac{(D_S - D_L)}{D_S D_L} \frac{4Gm}{c^2}} \tag{2.7}$$

Because the observer, lens, and source are aligned along the optic axis, the image is not a single point, but a ring of light around the lens. This ring is known as the Einstein ring with an angular radius θ_E known as the angular Einstein radius.

The typical mass of a lens in an observed microlensing event is on the order of the mass of our sun, i.e. a solar mass. Given a source star 8 kpc away from the earth, the angular Einstein radius of a solar mass lens 4 kpc away from earth is,[21]

$$\theta_E = \sqrt{\frac{(8 \text{ kpc} - 4 \text{ kpc})}{(8 \text{ kpc})(4 \text{ kpc})} \frac{4MG}{c^2}} \approx 1 \text{ milliarcsecond}$$

The Rayleigh criterion gives the minimum aperture size of a telescope required to resolve this Einstein ring to be

$$D = \frac{1.22\lambda}{\sin(2\theta_E)} \approx 60 \text{ m}$$

This is too large to be feasible, thus the Einstein rings in microlensing events are unobservable with current technology.

It is occasionally useful to consider the Einstein ring projected into the source sphere along with the physical Einstein radius instead of the angular radius. Projecting the Einstein ring into the source plane or the lens plane allows us to define the physical Einstein radius, as shown in Figure 2.3.

$$r_E = \theta_E D_L \quad \text{(Lens plane)} \tag{2.8}$$

$$\hat{r}_E = \theta_E D_S \quad \text{(Source plane)} \tag{2.9}$$

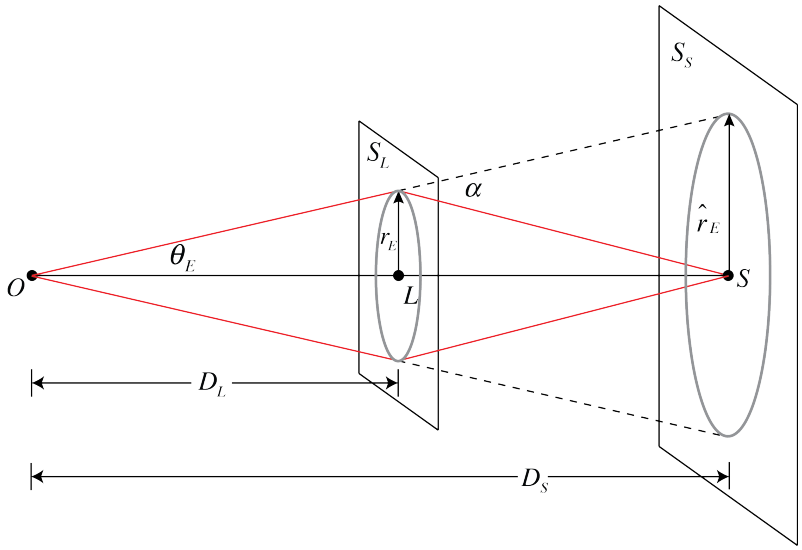

Figure 2.3: The Einstein Ring projected into the source plane S_S and the lens plane S_L.

While these distances have different physical lengths, they can be considered equivalent if the are measured relative to the Einstein radius within the respective plane.

2.4 Multiple Images

Relaxing the condition that $\beta = 0$ allows for the fact that microlensing events are unlikely to align as in the previous case. The geometry for the general case is only slightly more complicated than for the $\beta = 0$ case. Returning to the Equation 2.3 and plugging in the deflection angle, the lens equation can be written in the simple form, [25]

$$\theta^2 - \beta\theta - \theta_E^2 = 0 \tag{2.10}$$

Solving Equation 2.10 for any fixed position of the source $\beta \neq 0$ allows us to find values for the corresponding images the observer will see. The images will be at angular positions,

$$\theta_\pm = \frac{\beta}{2} \pm \theta_E \sqrt{1 + \frac{\beta^2}{4\theta_E^2}} \tag{2.11}$$

which correspond to two images of the source. The θ_+ will always be located outside of the Einstein Ring and θ_- will always be inside.[19] This is shown in Figure 2.4.

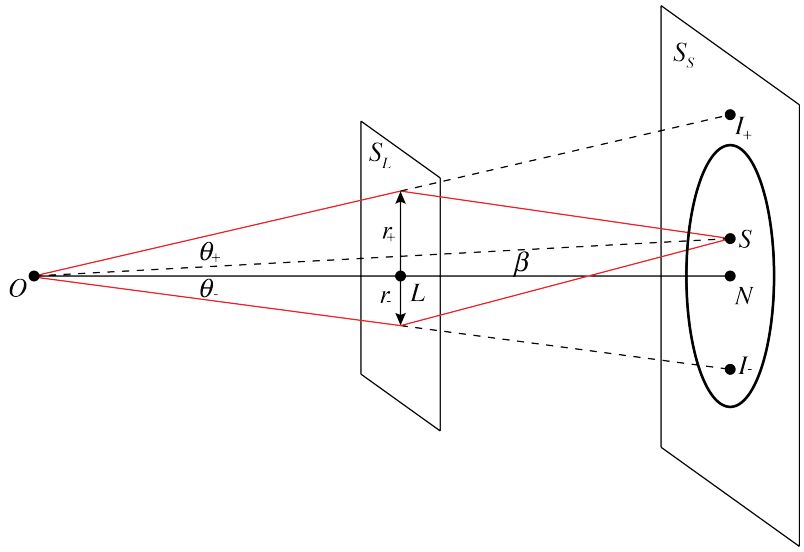

Figure 2.4: Two images, I_+ and I_-, are formed when $\beta > 0$. The first image is formed outside of the Einstein ring while the second is formed inside of the Einstein ring. The Einstein ring has been projected into the source plane for clarity.

The angular separation of the two images is given by,[21]

$$\triangle\theta = \theta_+ - \theta_- = 2\theta_E\sqrt{1 + \frac{\beta^2}{4\theta_E^2}} \tag{2.12}$$

hence when $\beta < \theta_E$, the difference between the images is on the order of the diameter of the Einstein ring and the images will not be observable.

2.5 Amplification

Thus far, we have discussed two modifications to the image of a light source that cannot be observed directly for lenses of interest to this thesis, i.e stars or planets. However, the deflection of light by a lens can produce a change in the apparent brightness of a source resulting from a distortion of the solid angle in which an object is seen.

The flux of an image of an infinitesimal source is the product of the surface brightness

of the source and the solid angle $d\Omega$ it subtends. Since the gravitational deflection of a light ray does not affect the surface brightness but does affect the shape of the solid angle, the flux will change as the light ray is deflected. This change in flux is observable. We define the amplification to be the ratio of the observed solid angle to the solid angle had no deflection taken place. [25][21]

$$A = \frac{d\Omega}{d\Omega_0} \tag{2.13}$$

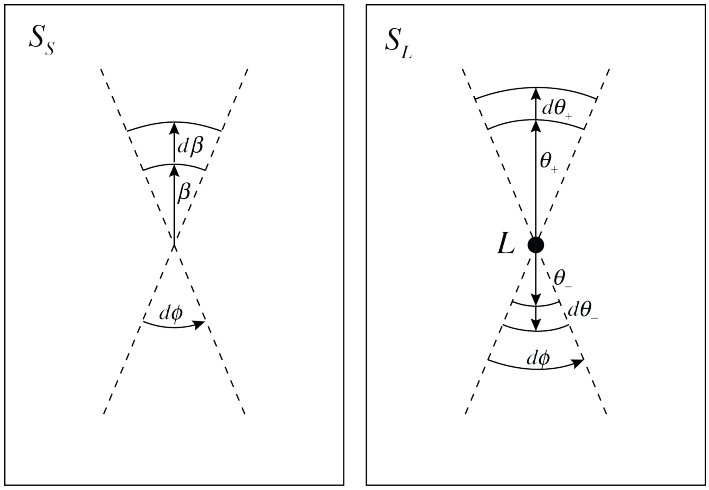

Figure 2.5: A surface element in polar coordinates on the source plane, S_S, is mapped to the lens plane, S_L resulting in two images.

In general, the solid angle is given as $d\Omega = dS/r^2$ where dS is the surface area of the solid angle and the r is the distance from the observer. From Figure 2.5, we can calculate

$$A_\pm = \frac{d\Omega}{d\Omega_0} = \frac{\theta_\pm d\theta_\pm}{\beta d\beta} \tag{2.14}$$

Using Equation 2.11, we find that,

$$A_\pm = \frac{1}{2} \pm \frac{\beta^2 + 2\theta_E^2}{2\beta\sqrt{\beta^2 + 4\theta_E^2}} \tag{2.15}$$

As stated previously, the images cannot be resolved. We can, however, find the overall

amplification from the two images.

$$A = |A_+| + |A_-| = \frac{\beta^2 + 2\theta_E^2}{\beta\sqrt{\beta^2 + 4\theta_E^2}} \tag{2.16}$$

As $\beta \to \infty$, $A_+ \to 1$ and $A_- \to 0$. Physically, this corresponds to the lens being far from the source and no amplification occurs. As $\beta \to 0$, the Total amplification diverges to infinity. This corresponds to when the lens is aligned with the source, producing an Einstein ring. In reality, observed microlensing events do not exhibit infinite amplification. This is an artifact of assuming a point source.[28] Assuming a finite source leads to a finite magnification and is discussed later.

2.6 Scaling the Parameters of a Microlensing Event

While the Einstein ring is not observable, we can treat the Einstein ring for a particular microlensing event as an intrinsic property of the lens. In other words, a lens has an associated angular Einstein ring radius, θ_E, regardless if the Einstein ring is formed or not and we can define the scale of microlensing events by normalizing the parameters involved with regard to θ_E. In doing so, we can simplify the equations we have discussed thus far.

We define the reduced angular lens-source separation u as

$$u = \frac{\beta}{\theta_E} \tag{2.17}$$

and the reduced image position y,

$$y = \frac{\theta}{\theta_E} \tag{2.18}$$

With these definitions, the angular Einstein ring radius is simply 1 for all microlensing events. The image positions are then given by,

$$y_\pm = \frac{u}{2} \pm \sqrt{1 + \frac{u^2}{4}} \tag{2.19}$$

and the total amplification by,

$$A = \frac{u^2 + 2}{u\sqrt{u^2 + 4}} \tag{2.20}$$

These definitions will be used for the remainder of this chapter.

2.7 Single Lens Light Curve

The amplification of a source star by a lens itself is not useful for determining if microlensing is taking place because we need to know the intensity of the star when the lens is not present. Luckily, objects in our galaxy are in constant motion which results in the source and lens having a relative velocity to each other.

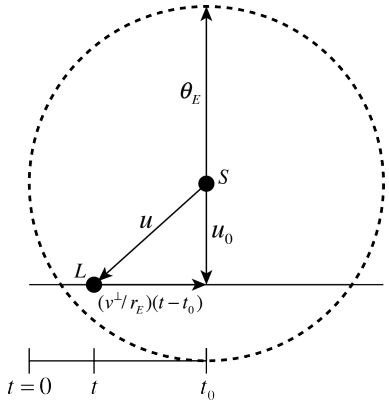

Figure 2.6: A lens, L, moves with some velocity $v_\perp$ perpendicular to an observer. The lens-source separation u changes with time. u_0 is the minimum lens-source separation.

Consider a lens moving with a perpendicular velocity $v_\perp$ relative to the observer, as depicted in Fingure 2.6. As the lens moves past the apparent position of the source star, the lens-source separation, u, changes in time. From Figure 2.6, we can write the lens-source separation in time as,[23]

$$u(t) = \sqrt{u_0^2 + \frac{{v_\perp}^2}{r_E}(t - t_0)^2} \tag{2.21}$$

where u_0 is the minimum lens-source separation and t_0 is the time when u_0 occurs. We can define a new parameter t_E as the time it takes the lens to move a distance equal to the

physical Einstein radius, r_E.[23]

$$t_E \equiv \frac{r_E}{v_\perp} \tag{2.22}$$

The parameter t_E sets the time scale of a microlensing event. Time scales of microlensing events can range from days to months, although typical events last for a few weeks. Combining the time scale, t_E, into Equation 2.21, u can be written as,

$$u(t) = \sqrt{u_0^2 + \left(\frac{t - t_0}{t_E}\right)^2} \tag{2.23}$$

As the lens moves across the sky, the images of the source move as well. Recall from Equation 2.19 that two images are produced, one inside the Einstein ring and one outside the Einstein ring. The path of the images is depicted in Figure 2.7. The Einstein ring is depicted by the dashed line. The source is positioned at the center of the Eisntein ring. The path of the lens is in blue while the images of the the source are in red.

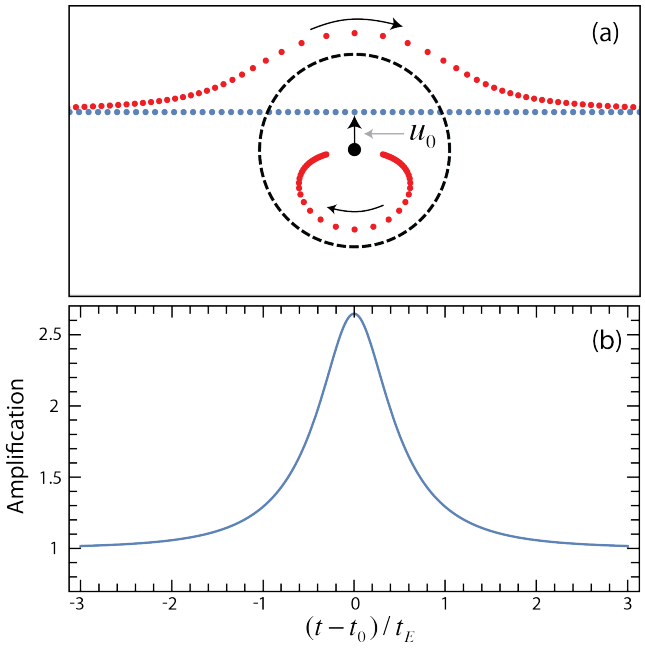

Figure 2.7: **(a)** A source (blue) moves across the sky with the lens centered at the origin. The images of the source (red) for each source position are shown. The arrows indicate the direction of the image motion as the source moves across near the lens. Two separate images are formed and move along the outside and inside of the Einstein ring. **(b)** A light curve corresponding to the source motion near a lens.

Thus far, we have assumed that the lens is in motion relative to the observer and the source. While this is physically true, it is conceptually useful to assume that the lens is stationary and that the source is in motion across the sky. Mathematically, nothing changes. Further discussion will assume this to be the case.

Combining Equation 2.23 with Equation 2.20 gives the time dependent amplification of the source. Figure 2.8 shows light curves for various minimum lens-source separations.

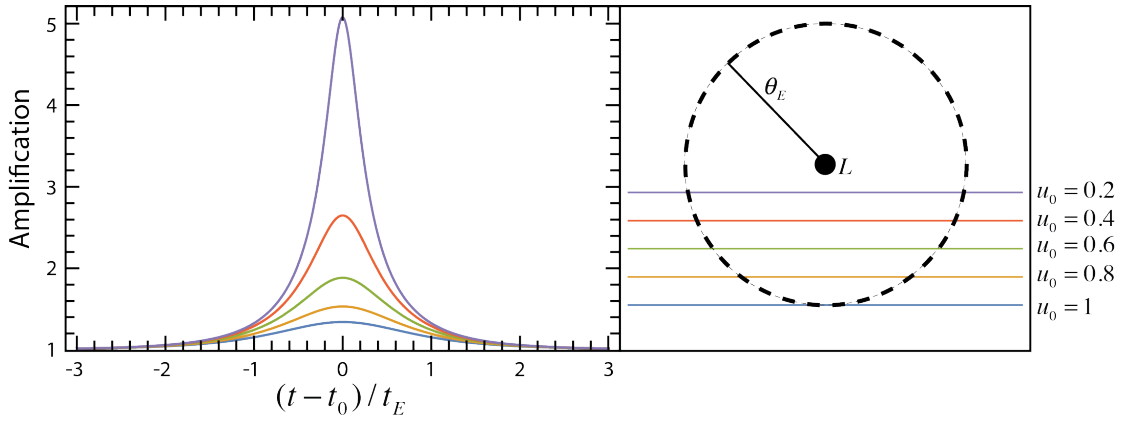

Figure 2.8: *Right*: The path of a lens moving across the sky for different minimum lens-source separations. *Left*:The light curve produced for different minimum lens-source separations. The colors of the curves correspond to the colors of lens path.

2.8 Observing a Microlensing Event

Microlensing events are quite rare. If we were to watch a single star, we would expect to wait roughly 100,000 years to see an event.[23] But, if we monitor 100 million stars simultaneously, we can expect to see many microlensing events a year. One such microlensing survey is conducted by the Optical Gravitational Lensing Experiment (OGLE) monitoring the galactic bulge where the star population is dense. The survey looks for an increase in intensity from a star and alerts observatories around the world of possible microlensing events. The data is then collected and fit using the single lens model described above.

Three parameters can be determined from fitting the data: the maximum amplification, A_{max}, the time of maximum amplification t_0, and the time scale of the event ,t_E. Of these

three parameters, only t_E is related to information about the lens itself. Unfortunately, t_E depends on the mass of the lens, relative velocity of the lens, and the distance to the lens in a convoluted way. Without direct knowledge of the distance to the lens and how fast it is moving, statistical methods must be used to determine a range of possible masses of the lens.

One of the first candidates for an observed microlensing events was recorded by the MACHO Project in 2003.[2] The group observed the event in two different light spectra, red (630nm - 760nm) and blue (450nm - 630nm). They found $A_{max} = 6.68 \pm 0.11$, $t_0 = 433.55 \pm 0.04$ days, and $t_E = 33.0 \pm 0.26$ days. Figure 2.9 shows the data collected.

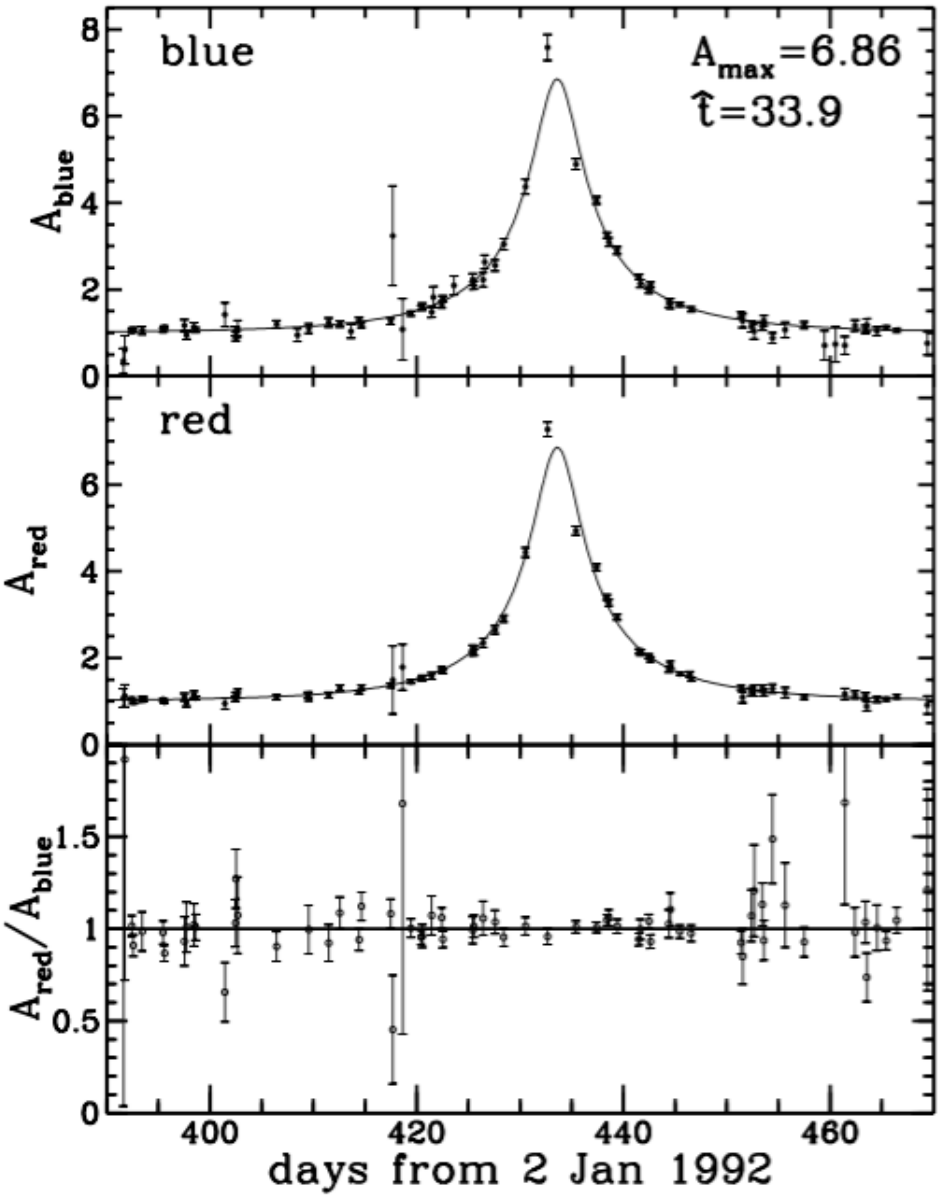

Figure 2.9: Top panel shows light amplification data for blue bandpass (450nm - 630nm). The smooth curve is the best-fit amplification model derived previously. $\hat{t}$ corresponds to t_E in the notation used for this thesis. The middle panel is the same for red bandpass (630nm - 760nm). The bottom panel is the color light curve, showing the ratio of red to blue flux, normalized so that the median is unity.

Chapter 3

Breaking the Microlensing Degeneracy

In Chapter 2, we described the light curve produced by a point source star being lensed by a point lens. From the light curve, we can determine A_{max}, t_0, and t_E. The time scale, t_E, is the only parameter that contains any information about the lens itself, but it is related to the physical characteristics of the lens in a convoluted way leading to a degeneracy. While the simple microlensing model outlined previously describes a majority of microlensing events, some observed events deviate dramatically from the light curve discussed in Chapter 2.

These deviations occur when one or multiple assumptions used in deriving the single lens amplification breaks down. The resulting light curves are generally classified as anomalous. By measuring these anomalies, it is possible to break at least some of the degeneracy in t_E. The rest of this thesis will be devoted to three of the most common sources of anomalies; finite source effects in high magnification events, parallax measurements, and binary lenses. Binary lenses will be discussed in chapter 4. This Chapter will be devoted breaking the microlensing degeneracy by measuring finite source effects in high magnification events. In addition, space-based satellite parallax effects will be discussed.

3.1 Finite Source Effects

As previously mentioned, the assumption of a point source leads to diverging amplification as $u_0 \to 0$. Of course, stars in our galaxy are not point sources and their physical size becomes important as lens-source separation u_0 becomes small enough that the lens passes over the face of the star. By taking the size of the star into account, it becomes possible to measure the angular Einstein radius, θ_E. Measurements of θ_E are important because of the constraint it puts on the physical properties of the lens. Recall that we defined the time scale of the event, t_E, as,

$$t_E \equiv \frac{r_E}{v_\perp} = \frac{D_L \theta_E}{v_\perp} \tag{3.1}$$

We define a new parameter, the relative velocity of the source, $\mu_{rel} \equiv v_\perp / D_L$.[13] With this definition and Equation 3.1, we can rewrite θ_E as,[32]

$$\theta_E = \mu_{rel} t_E \tag{3.2}$$

By measuring t_E and θ_E from an observed light curve, we can calculate μ_{rel}. The question becomes how we go about calculating θ_E from a light curve involving finite source effects. We begin by treating the star as a disk.[28] The star has some angular radius, θ_*, which can be measured from the source star's temperature and Stefan-Boltzmann law, and thus is assumed to be a known quantity.[14] By normalizing the size of the star to the angular Einstein radius, we define a normalized angular radius of the star, ρ, as,

$$\rho \equiv \frac{\theta_*}{\theta_E} \tag{3.3}$$

For simplicity, we assume that the surface brightness is constant across the face of the star. As the source moves across the sky, the lens passes over the face of the star, as depicted

in Figure 3.1. Consider the amplification of a single point on the face of the star, given by

$$A(u') = \frac{u'^2 + 2}{u'\sqrt{u'^2 + 4}} \tag{3.4}$$

where u' is the separation of the lens from the point. We can relate u' to the center of the disk by using the law of cosines to give,

$$u' = u^2 + r^2 - 2ur\cos\phi \tag{3.5}$$

where u is the distance of the lens from the the center of the source, r is the distance to the point from the center of the source, and ϕ is the angle between u and r as depicted in Figure 3.1. By averaging the amplification over the entire face of the star, we can calculate

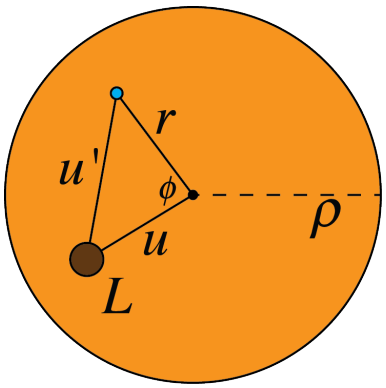

Figure 3.1: Shows a lens L passing over the face of a star in which the size of the star must be taken into account. A star is assumed to be a disk with a reduced radius, ρ.The lens source separation, u, is defined from the center of the star. The separation, u', is the lens source separation of the lens and an arbitrary point on the star. r is the distance between the arbitrary point and the center of the star and ϕ is the angle between u and r.

the total amplification of the source. We integrate the amplification $A(u')$ over the entire face of the star, and then divide by the area of the star to give the total amplification, A^*, of the source.

$$A^*(u,\rho) = \frac{\int_S A(u')dS}{\int_S dS} = \frac{1}{\pi\rho^2}\int_0^{2\pi} d\phi \int_0^{\rho} rA[u^2 + r^2 - 2ur\cos\theta]dr \tag{3.6}$$

Because the source is in motion, the amplification will depend on time as,

$$u'(t) = \sqrt{u_0'^2 + \left(\frac{t - t_0}{t_E}\right)^2}$$

where u_0' is the minimum separation between the lens and the point of interest in Figure 3.1. The light curve produced by a finite source differs greatly from that of the point source light curve when the lens source separation is on the order of the size of the source. For small u_0, instead of the amplification diverging, the light curve is smoothed out, as depicted in Figure 3.2.

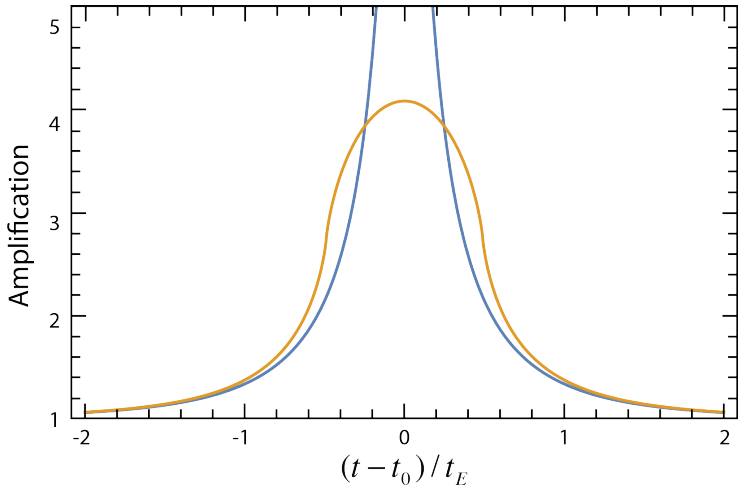

Figure 3.2: An example of the light curve produced when the finite size of a star is taken into account is shown by the orange curve. The blue curve is the point-source light curve described in chapter 1.

The central region of the light curve contains information about how long it takes the lens to pass across the face of the source star. The turning points of the light curve correspond to when the lens enters and exits the face of the star and thus we find the time it takes the lens to traverse the source, T, to be the time between these turning points on the curve.[22] Relating T to other variables of interest is done by examining the geometry of the problem, depicted in Figure 3.3.

The source is moving across the sky with a velocity $v_\perp$. The time it takes the lens to traverse halfway across the face of the star is $T/2$. Thus we can relate the normalized radius

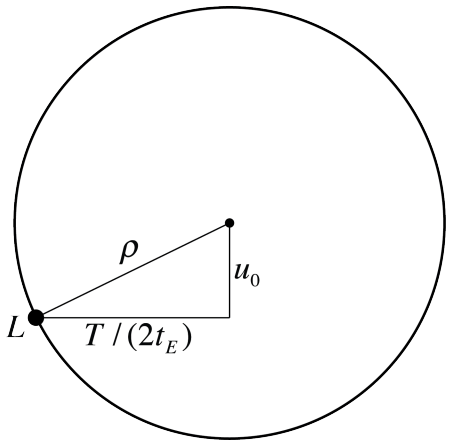

Figure 3.3: Geometry of the lens L passing over the face of the star. From this geometry, we can solve for T, the time for the lens to cross the face of the star.

of the star, ρ, to T by,[18][6]

$$T = 2t_E\sqrt{\rho^2 - u_0^2} \tag{3.7}$$

where t_E and u_0 are determined from the overall shape of the curve, as in the points source case. Combining Equations 3.1 and 3.7, θ_E is calculated by,

$$\theta_E = \theta_* \left[\left(\frac{T}{2t_E} \right)^2 + u_0^2 \right]^{-1/2} \tag{3.8}$$

To be more precise, the assumption that a star has constant surface brightness is not exactly true, as a real star is brightest near the center and darkens on the outer limb. This effect is known as "limb darkening" and should be taken into account when making microlensing measurements. Stars will have different brightness profiles, and the profile can be determined by fitting different models of limb darkening to microlensing data.

The first observation of finite source effects in a microlensing event was observed by Global Microlensing Alert Network (GMAN) and analyzed by Alcock et al.[1] They analyzed the light curve using the point source model described in Chapter 2, the constant brightness model described in this section, and a limb darkening model. Figure 3.4 shows the observed light curve and Figure 3.5 shows the results for the three fit models.

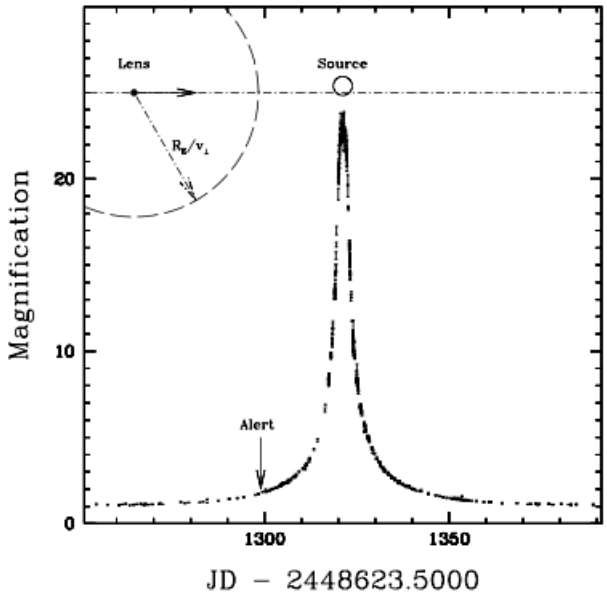

Figure 3.4: An observed event by Alcock et al.[1] This event was the first event observed in which finite source effects needed to be taken into account. The dashed line shows the trajectory of the lens over the source star. The observation data is shown without a best fit line.

MACHO Alert 95-30 Microlensing Statistics

Fit[a]	t_0 [b]	$\hat{t}$[c]	$u_{\min}$	u_*	ω[d]
1.....	1321.2 (1)	67.70 (13)	0.04069 (12)	0	?
2.....	1321.2 (1)	67.36 (1)	0.05579 (1)	0.07335 (1)	22.1 (30)
3.....	1321.2 (1)	67.28 (27)	0.05408 (20)	0.07561 (9)	21.5 (29)

Figure 3.5: Table of measured parameters from a finite source event analyzed by Alcock et al.[1]

3.2 Microlensing Parallax

The simple light curve described in Chapter 1 also assumes that the motion of the earth is constant with respect to source star. While this assumption holds for microlensing events with short duration, during a long microlensing event (on the order of a couple of months), the earth's motion around the sun becomes important. The earth's orbital motion produces a parallax effect with respect to the lens and the source star, resulting in an asymmetric light curve. One such light curve was observed by Alcock et. al, depicted in Figure 3.6.[3]

As with finite source effects, parallax effects allow for further degeneracy breaking from the simple light curve. However, because microlensing events are typically on the order of a few weeks, not months, observing the parallax effect due to the Earth's orbital motion is quite rare.

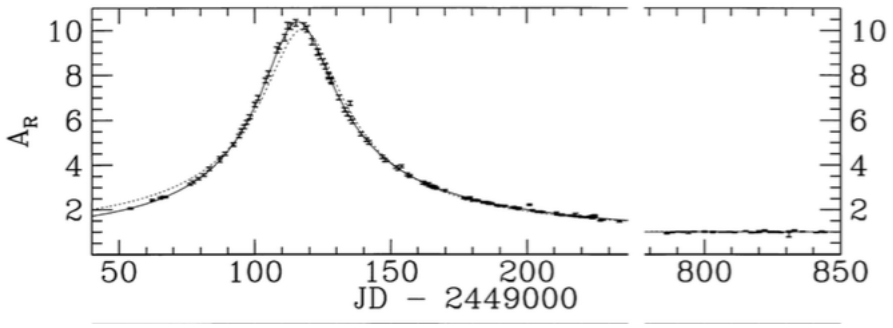

Figure 3.6: A microlensing parallax event observed by Alcock et al.[3] caused by the earths rotation around the sun. The best fit curve is shown by the black curve, while the basic microlensing light curve is shown by the dashed curve for reference.

It is possible to create a parallax effect by observing an event simultaneously from two positions. This is typically done by observing a microlensing event using a satalite, as was suggested by Refsdal in 1966, although it is sometimes possible to observe parallax effect in very high magnification events from two positions on Earth.[24][11] Refsdal concluded that if a microlensing event could be observed from at least two separate locations, the mass and distance to the lens could be constrained. This is because light curves observed from different perspectives will differ in magnification, but will have the same Einstein crossing time. Thus, comparing the light curves from different positions allows for a determination in the parameters of interest.[17]

Gould suggested parallax measurements could be used to measure the radius of the Einstein ring projected into the observer plane.[12] To project the Einstein radius into the observer's plane, it is useful to reverse the geometry used in Chapter 2, as depicted in Figure 3.7.[15]

From Figure 3.7, we can relate the physical Einstein radius in the observer plane, $\tilde{r}_E$, to

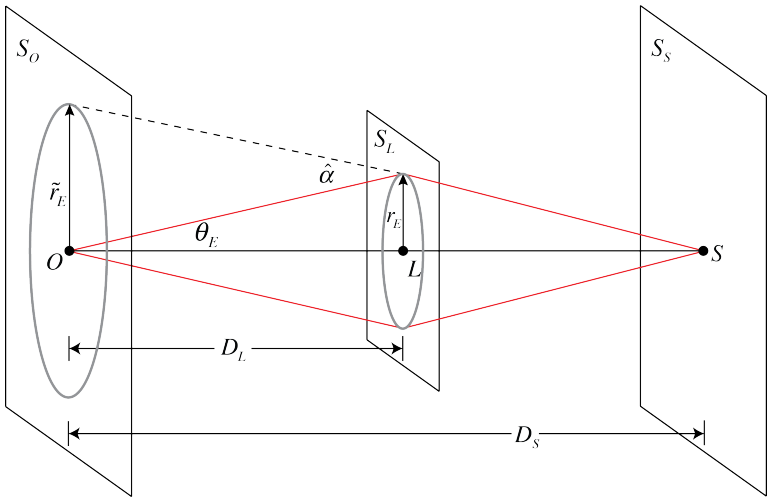

Figure 3.7: Shows the geometry of projecting the physical Einstein ring radius, r_E, from the lens plane into the observer plane. The physical Einstein ring radius projected into the observer plane is denoted $\tilde{r}_E$.

the Einstein radius in the lens plane, r_E, and source plane by,

$$\tilde{r}_E = \frac{D_S}{(D_S - D_L)} r_E = \frac{D_L}{(D_S - D_L)} \hat{r}_E \tag{3.9}$$

As Gould suggested, the parallax effect can be used to determine $\tilde{r}_E$ of a particular event. Consider a satellite in the observer plane positioned at some distance d_{sat} away from Earth. The light curve observed from the satellite will differ from the light curve observed from the Earth, as shown in Figure 3.8. This is due to the fact that the satellite is viewing the event from a different angle than that of the Earth which causes a different lens-source separation. We will denote the lens-source separation from the Earth and the satellite as the two dimensional vectors $\vec{u}(t)$ and $\vec{u}'(t)$, respectively. Figure 3.9 shows the different trajectories of the source as it passes near the lens as seen from the Earth and the satellite. The addition of a second observer allows measurement of the separation between these two trajectories. We denote the trajectory separation, $\Delta\vec{u}$, defined as,[12]

$$\Delta\vec{u} = \vec{u}'(t) - \vec{u}(t) \tag{3.10}$$

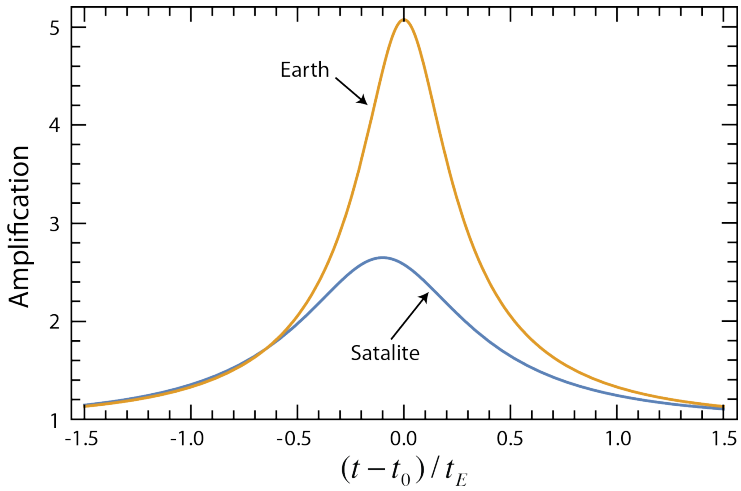

Figure 3.8: Example of the difference in observed light curves by the Earth (orange) and a satellite (Blue).

We can write the individual lens-source separations as,[12]

$$\vec{u}(t) = \vec{u}_0 + \frac{(t-t_0)}{r_E}\vec{v_\perp}, \qquad \vec{u'}(t) = \vec{u'_0} + \frac{(t-t'_0)}{r_E}\vec{v_\perp} \tag{3.11}$$

where $\vec{v}_\perp$ is the velocity of the source perpendicular to the observer plane. We cannot determine the vectorial trajectory separation, $\Delta\vec{u}$, from the light curves. However, we can determine the maginitude of the trajectory separation by,

$$\Delta u = \sqrt{(\Delta u_0)^2 + (\Delta t_0)^2} \tag{3.12}$$

where $\Delta u_0 = u'_0 \pm u_0$ and $\Delta t_0 = (t'_0 - t_0)/t_E$ and $t_E = r_E/v_\perp$. Because u_0, u'_0, t_0, t'_0, and t_E are determined from the individual light curves, Δu can be determined. There is a two fold degeneracy in the measurement of Δu arising from two possible minimum lens-source separations because we have no way of determining whether the two trajectories of the source occur on the same side or opposite sides of the lens, as shown in Figure 3.9. This degeneracy can be completely resolved if the event is observed by a second satellite. This is because the comparison of the light curves between the earth and the second satellite will produce two values of Δu_0, only one of which will agree with the values obtained from Earth and the first

satellite.

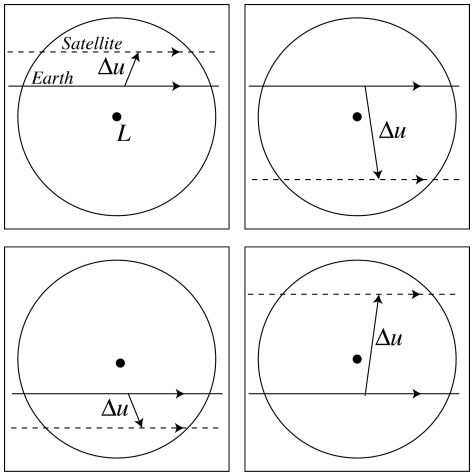

Figure 3.9: Shows four possible trajectories of the source near a lens as observed by the Earth and a satellite. These four possibilities result in a 4-fold degeneracy of $\Delta\vec{u}$. The magnitude, Δu has 2-fold degeneracy.

We can also write $\Delta\vec{u}$ in terms of the satellite Earth separation $\vec{d}_{sat}$. From the geometry shown in Figure 3.10, we can relate $\vec{d}_{sat}$ to $\Delta\vec{u}$ by,

$$\vec{\phi} = \frac{\vec{d}_{sat}}{D_L} = -\frac{\hat{r}_E \Delta\vec{u}}{(D_S - D_L)} \tag{3.13}$$

Taking the magnitude of Equation 3.13, we can write,[12]

$$\frac{d_{sat}}{\Delta u} = \tilde{r}_E \tag{3.14}$$

Thus, with knowledge of how far away our satellite is from earth, we can determine Δu using the observed light curves from the Earth and the satellite and then measure the physical Einstein radius projected into the observer plane.

The first space-based microlens parallax measurement was observed using the Spitzer telescope in 2014 and analyzed by Yee et.al.[31] Figure 3.11 shows the data collected from ground based observatories and Spitzer. The source star was located within the galactic disk, thus an approximate velocity of 250 km/s could be estimates for the star. Under

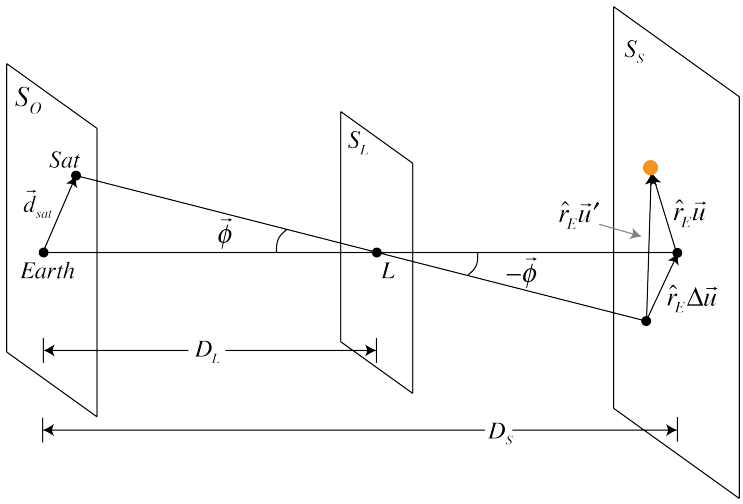

Figure 3.10: The geometry of a space based parallax event. A satellite is a distance $\vec{d}_{sat}$ from the earth in the lens plane. The apparent lens-source separation as perceived by the Earth is $\vec{u}$, while the apparent lens-source separation as perceived by the satellite is $\vec{u}'$. Multiplying by $\hat{r}_E$ projects the lens-source separation from each into the source plane. The difference in the apparent lens-source separations is $Delta\vec{u}$.

this assumption, the mass of the lens and the distance to the lens were estimated to be $m = 0.23 \pm 0.07 M_\odot$ and $D_L = 3.1 \pm 0.4$ kpc, respectively.

3.3 Complete Solutions to a Microlensing Event

While the mass and distance to the lens can be constrained by assuming the velocity of the lens based on where the source star is located in the galaxy, for some events, as was done by Yee et. al., it is possible to determine all of the parameters directly from observation. In the previous sections, we have developed methods for determining θ_E in high magnification events and $\tilde{r}_E$ in all events with the use of satellites. If satellites are used observe high magnification events, we can measure both θ_E and $\tilde{r}_E$ for the a single event, allowing us to directly calculate the mass of the lens by,

$$\theta_E \tilde{r}_E = \frac{4Gm}{c^2} \tag{3.15}$$

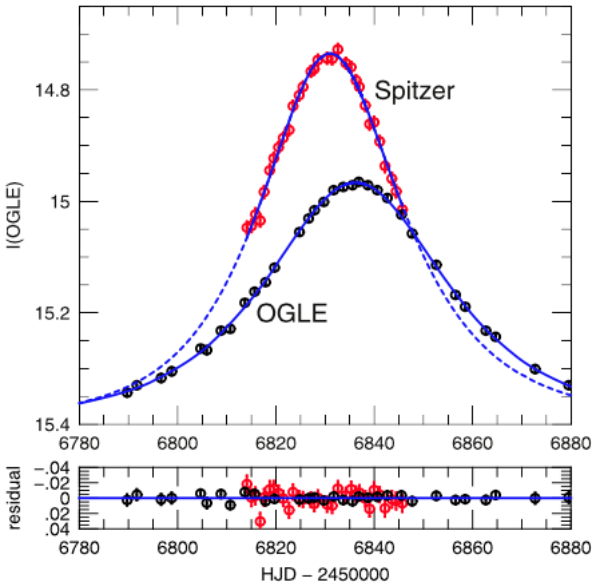

Figure 3.11: A microlensing event as seen from the Earth (observation data shown in blue) and the Spitzer satellite (observation data shown in red). Dashed blue line shows the best fit curve extended outside the observation range of the Spitzer satellite.

In addition, the distance to the lens can be resolved with knowledge of the distance to the source star by equation 3.9,

$$\tilde{r}_E = \frac{D_S}{(D_S - D_L)} r_E = \frac{D_S D_L}{(D_S - D_L)} \theta_E$$

The velocity of the lens is found from the relative velocity,

$$\mu_{rel} = \frac{\theta_E}{t_E} = \frac{v_\perp}{D_L}. \tag{3.16}$$

Zhu et al. observed one such event. Figure 3.12 shows the data collected from earth observatories and by the Spitzer telescope, along with the best fit curves.[33] The light curve from earth was seen as a high magnification event, while the light curve from Spitzer had a comparatively large minimum lens source separation. The mass of the lens $45 \pm 7 M_J$, where M_J is a Jupiter mass. The distance to the lens was found to be 5.9 ± 1.9 kpc. This star is determined to be a brown dwarf star.

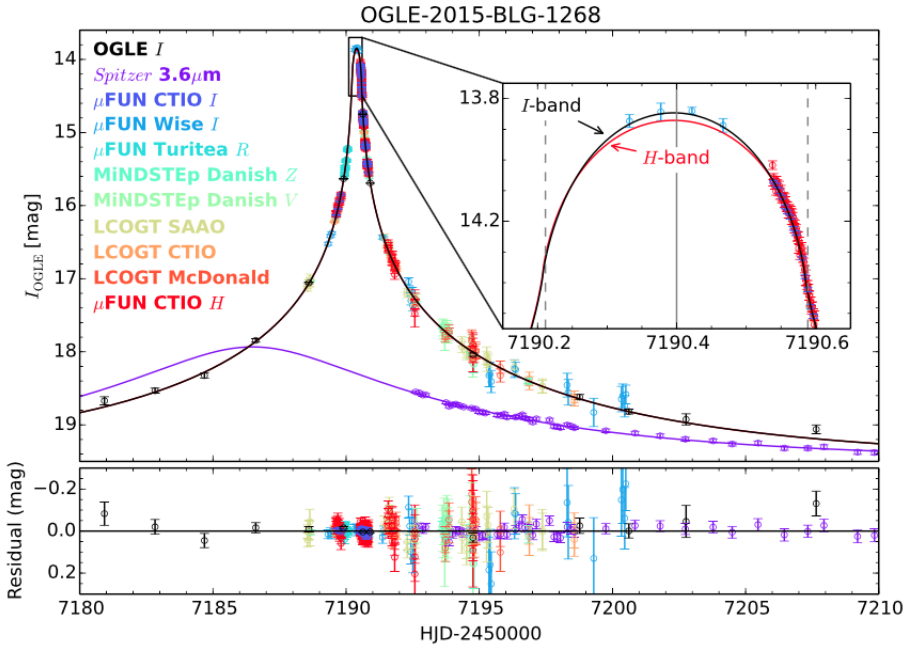

Figure 3.12: A high magnification event observed from earth and the Spitzer satellite observed by Zhu et al.[33]

Chapter 4

Exoplanetary Microlensing

Today, microlensing is primarily used to detect planets. We have seen that as a source moves relative to a lens, the images of the source move as well. If the lens is a binary system consisting of a star and a planet, the image of the source star may coincide with the position of the planet. The image of the source is essentially lensed a second time, producing a significant deviation to the single lens light curve discussed thus far. It is these deviations to the light curve that allow microlensing to be used to detect planets.

The addition of a second mass to the lens increases the complexity considerably because it adds additional parameters to the lens equation, namely the mass ratio of the lens, q, and the star-planet separation, d, and the angle the source moves across the sky relative to the lens-star axis, ϕ. In this section, we discuss the formulation of a general lens equation for N lenses, and give a detailed description of binary lens systems. We then discuss how measurements of the mass ratio and the star-planet separation can be measured from the light curve.

4.1 General Lens Equation

Because the the deflection angle of light passing near a massive object depends linearly on the mass, the deflection angle can be linearly superimposed. This enables us to write the

general lens equation for N point masses located in the lensing plane.

In order to see how this works in practice, consider a binary lens system consisting of two lenses m_1 and m_2, where m_1 is a distance D_L from the observer. We define the lens plane as the plane passing through m_1 perpendicular to the observer. The position of m_2 is projected into the lens plane and a coordinate system (y_1, y_2) is defined. This allows us to write the position of the lenses in the lens plane as the vectors $\vec{\theta}_1$ for m_1 and $\vec{\theta}_2$ for m_2. [27]

The source plane is defined as the plane through a source star a distance D_S from the observer perpendicular to the optic axis, i.e perpendicular to the a line from the observer through the origin of the lens plane. We define a coordinate system (u_1, u_2) in the source plane such that it is parallel to the coordinate system in the lens plane. The origin of this coordinate system is the intersection of the optic axis in the source plane. The position of the source is given by the vector $\vec{\beta}$.

A light ray originating from the source and passing through the lens plane will be deflected by some amount. Because the the deflection angle of light passing near a massive object depends linearly on the mass, the deflection angle can be linearly superimposed.[26] This means the total deflection angle of the light ray passing through the lens plane is the sum of the deflection angles of the individual masses. In terms of the coordinate system defined in the lens plane, for a light ray intersecting the lens plane at a position $\vec{\theta}$, the total deflection angle is given by

$$\hat{\vec{\alpha}}(\vec{\theta}) = \frac{4Gm_1}{c^2 D_L}\frac{\vec{\eta_1}}{|\vec{\eta_1}|^2} + \frac{4Gm_2}{c^2 D_L}\frac{\vec{\eta_2}}{|\vec{\eta_2}|^2} = \frac{4Gm_1}{c^2 D_L}\frac{\vec{\theta}-\vec{\theta}_1}{|\vec{\theta}-\vec{\theta_1}|^2} + \frac{4Gm_2}{c^2 D_L}\frac{\vec{\theta}-\vec{\theta}_2}{|\vec{\theta}-\vec{\theta_2}|^2}$$

The lens equation is written as

$$\vec{\beta} = \vec{\theta} - \frac{D_S - D_L}{D_S}\hat{\vec{\alpha}}(\vec{\theta})$$

Defining $\vec{\alpha}(\vec{\theta}) = \frac{D_S D_L}{D_S - D_L}\frac{c^2}{4G}\hat{\vec{\alpha}}(\vec{\theta})$, the lens equation becomes,

$$\vec{\beta} = \vec{\theta} - \vec{\alpha}(\vec{\theta}) = \vec{\theta} - m_1\frac{\vec{\theta} - \vec{\theta}_1}{|\vec{\theta} - \vec{\theta}_1|^2} - m_2\frac{\vec{\theta} - \vec{\theta}_2}{|\vec{\theta} - \vec{\theta}_2|^2}$$

This can be further generalized to N lenses as,

$$\vec{\beta} = \vec{\theta} - \sum_i^N m_i\frac{\vec{\theta} - \vec{\theta}_i}{|\vec{\theta} - \vec{\theta}_i|^2}$$

We can normalize the angles in the lens equation with respect to the angular Einstein radius defined as,

$$\theta_E \equiv \sqrt{\frac{(D_S - D_L)}{D_S D_L}\frac{4GM}{c^2}} \tag{4.1}$$

where $M \equiv \sum m_i$ is the total mass of the lensing system. By making the following definitions,

$$\vec{u} = \frac{\vec{\beta}}{\theta_E}, \qquad \vec{y} = \frac{\vec{\theta}}{\theta_E}, \qquad \epsilon_i = \frac{m_i}{M}$$

we can write the lens equation as

$$\vec{u} = \vec{y} - \sum_i^N \epsilon_i\frac{\vec{y} - \vec{y}_i}{|\vec{y} - \vec{y}_i|^2} \tag{4.2}$$

where $\vec{u}$ is the source position relative to the optic axis (or angular lens-source separation) $\vec{y}$ is the position of the image, and $\vec{y}_i$ are the positions of the lens in the lens plane relative to the origin. The lens equation can be written as an $N + 2$ degree polynomial and therefore solving the lens equation gives $N + 2$ image locations. We solve the lens equation for $N = 2$, i.e., the binary lens, below.

4.2 Amplification of Multiple Lenses

The lens equation can be thought of as a two dimensional mapping between the position of the source and the positions of the images. The Jacobian of this mapping is given by,

$$\det J = \det\left(\frac{\partial \vec{u}}{\partial \vec{y}}\right) = \det\begin{pmatrix} \frac{\partial u_1}{\partial y_1} & \frac{\partial u_1}{\partial y_2} \\ \frac{\partial u_2}{\partial y_1} & \frac{\partial u_2}{\partial y_2} \end{pmatrix}$$

Recall that we defined the amplification of the source due the microlensing as the ratio of the solid angle of the source in the lens plane to the solid angle in the source plane,

$$A = \frac{d\Omega}{d\Omega_0}$$

This is because the shape of the solid angle changes due to different points along the solid angle being deflected by slightly different angles along the surface. This causes a warping of the solid angle in the lens plane. The amount that the area of the solid angle changes as it passes through the lens plane is given by the determinant of the Jacobian. In other words, we can relate the size of the solid angle in the source plane to the size of the solid angle in the lens plane by $d\Omega_0 = \det J d\Omega$. The amplification of the source is then given by

$$A_j = \left.\frac{1}{\det J}\right|_{z=z_j} \tag{4.3}$$

where A_j is evaluated at the position of a particular image position z_j. As with the single lens, the individual images are not observable and, instead we will be interested in the total amplification of the images. This is given by,

$$A = \sum_j^N |A_j| \tag{4.4}$$

As the lens system moves near the line of sight of the source star, the amplification will change producing a light curve. This light curve will differ drastically from the light curve we discussed in section 2.

4.3 Complex Coordinates

It is common practice to write the lens equation in complex coordinates instead of the vector coordinates we defined above.[30] Defining $\vec{u} = (u_1, u_2)$ and $\vec{y} = (y_1, y_2)$, we can redefine these coordinates into complex coordinates as,

$$\zeta = u_1 + iu_2$$

$$z = y_1 + iy_2$$

and rewrite the lens equation to give,

$$\zeta = z - \sum_{i}^{N} \frac{\epsilon_i}{\bar{z} - \bar{z}_i} \tag{4.5}$$

where $\bar{z}$ is the complex conjugate of z which arise from the identity,

$$\frac{z}{|z|^2} = \frac{z}{z\bar{z}} = \frac{1}{\bar{z}} \tag{4.6}$$

By solving for z we can find the positions of the images produced by the lenses, as was done with the single source previously. This is done by rewriting the lens equation as a complex polynomial. This results in a $(N^2 + 1)$ order complex polynomial which is only solvable analytically for $N = 1$. Numerical techniques must be used in order to solve for the image positions for $N > 1$.

The determinant of the Jacobian in complex coordinates takes the form,[30]

$$\det J = \det \begin{pmatrix} \frac{\partial \zeta}{\partial z} & \frac{\partial \zeta}{\partial \bar{z}} \\ \frac{\partial \bar{\zeta}}{\partial z} & \frac{\partial \bar{\zeta}}{\partial \bar{z}} \end{pmatrix} = \left| \frac{\partial \zeta}{\partial z} \right|^2 - \left| \frac{\partial \zeta}{\partial \bar{z}} \right|^2 . \tag{4.7}$$

Combining with Equation 4.5 gives,

$$\det J = 1 - \left| \frac{\partial \zeta}{\partial \bar{z}} \right|^2 \tag{4.8}$$

An important property of microlensing (and gravitational lensing in general) is that some source positions can result in a diverging amplification. From Equation 4.3, this occurs when the Jacobian is equal to zero or when,

$$\left| \frac{\partial \zeta}{\partial \bar{z}} \right|^2 = 1. \tag{4.9}$$

The possible image positions in which this is true are given by,

$$\frac{\partial \zeta}{\partial \bar{z}} = e^{i\phi} \tag{4.10}$$

where ϕ ranges from 0 to 2π. The set of curves created by solutions to Equation 4.10 define a set of curves in the lens plane known as critical curves. Mapping the critical curves to the source plane produces what are known as caustic curves. The importance of caustic curves in multi-lens systems cannot be overstated, and will be discussed in more detail below.

4.4 Binary Lens

The binary lens is of particular interest because of the ability to use microlensing to find exoplanets orbiting around a lens. The lens equation for a binary system is given by,

$$\zeta = z - \frac{\epsilon_1}{\bar{z} - \bar{z_1}} - \frac{\epsilon_2}{\bar{z} - \bar{z_2}} \tag{4.11}$$

The amplification of a particular image is found by Equation 4.8. The critical curves for a binary lens are found by solving Equation 4.10 which has the form,

$$\frac{\partial \zeta}{\partial \bar{z}} = \frac{\epsilon_1}{(\bar{z} - \bar{z_1})^2} + \frac{\epsilon_2}{(\bar{z} - \bar{z_2})^2} = e^{i\phi} \tag{4.12}$$

Conjugating Equation 4.12 and clearing the fractions, we obtain a 4th order polynomial in z,

$$\epsilon_1(z - z_2)^2 + \epsilon_2(z - z_1)^2 = (z - z_1)^2(z - z_2)^2 e^{-i\phi} \tag{4.13}$$

Solving Equation 4.13 for values of ϕ ranging from 0 to 2π produces the the possible positions of the images in the lens plane where the source appears infinitely magnified, known as critical curves. The positions of the source are found by mapping the critical curves back to the source plane, Equation 4.11, producing the caustic curves.

A binary system has one, two, or three closed caustic curves. Which of these three possibilities is exhibited depends on the mass ratio and separation of the of the binary system, defined as,

$$q \equiv \frac{\epsilon_1}{\epsilon_2} = \frac{m_1}{m_2}, \qquad d \equiv |z_1 - z_2| \tag{4.14}$$

where m_1 and m_2 are the actual masses of the two objects. Figure 4.3 shows how the star source separation d, affects the shape of the critical and caustic curves , while Figure 4.4 shows how critical and caustic curves when the mass ration q changes.

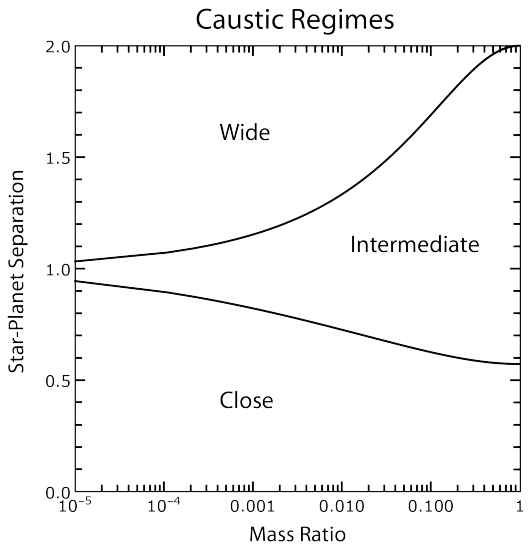

Figure 4.1: The regimes of a binary microlensing event are shown with respect to the mass ratio q and the star-planet separation d. The curves depict the boundary between each regime.

The three possible caustic topologies can be classified into regimes called "close", "intermediate", and "wide" binary systems.[27] For a given mass ratio, q, the value of d for which the regime changes from close to intermediate is defined by, [9]

$$\frac{q}{(1+q)^2} = \frac{(1-d_c)^2}{27d_c^8} \tag{4.15}$$

and the value of d for which the regime changes from intermediate to wide is defined by

$$d_w = \frac{(1+q^{1/3})^{3/2}}{\sqrt{1+q}} \tag{4.16}$$

For $d < d_c$, this defines the close regime and produces two closed caustic curves, for $d_c \leq d < d_w$, this defines the intermediate regime and produces one closed caustic curve, and for $d > d_w$ this defines the wide regime and produces three closed caustic curves. The three caustic regimes are depicted in Figure 4.1 where Equations 4.15 and 4.16 determine the boundary between each region. When $q = 1$, the critical values of the separation are $d_c = 2^{-1/2}$ and $d_w = 2$. The critical and caustic curves in these cases are shown in Figure

4.2.

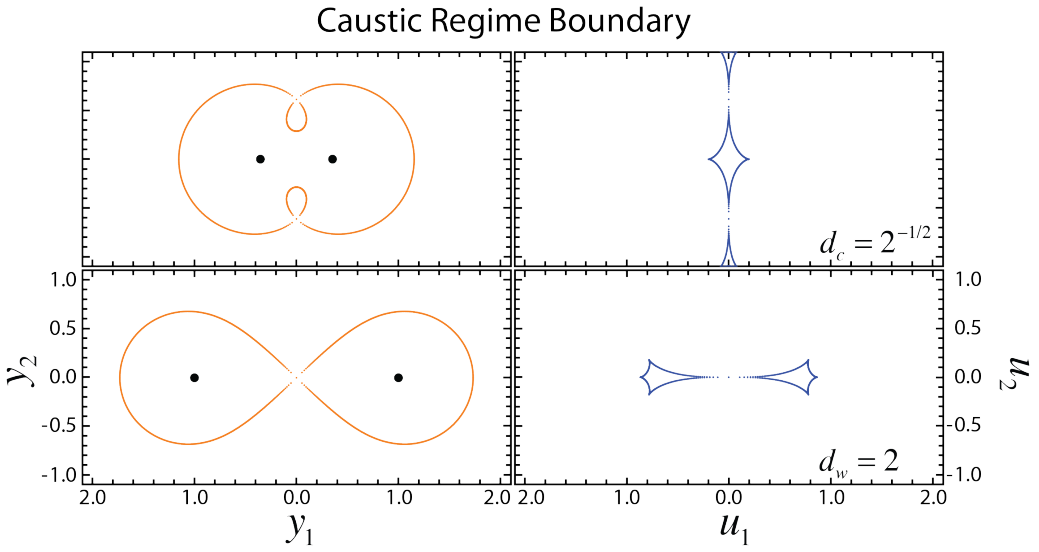

Figure 4.2: Critical and caustic curves when the star-planet separation is equal to the critical values,$d = d_W$ and $d = d_C$. The mass ratio is set to $q = 1$.

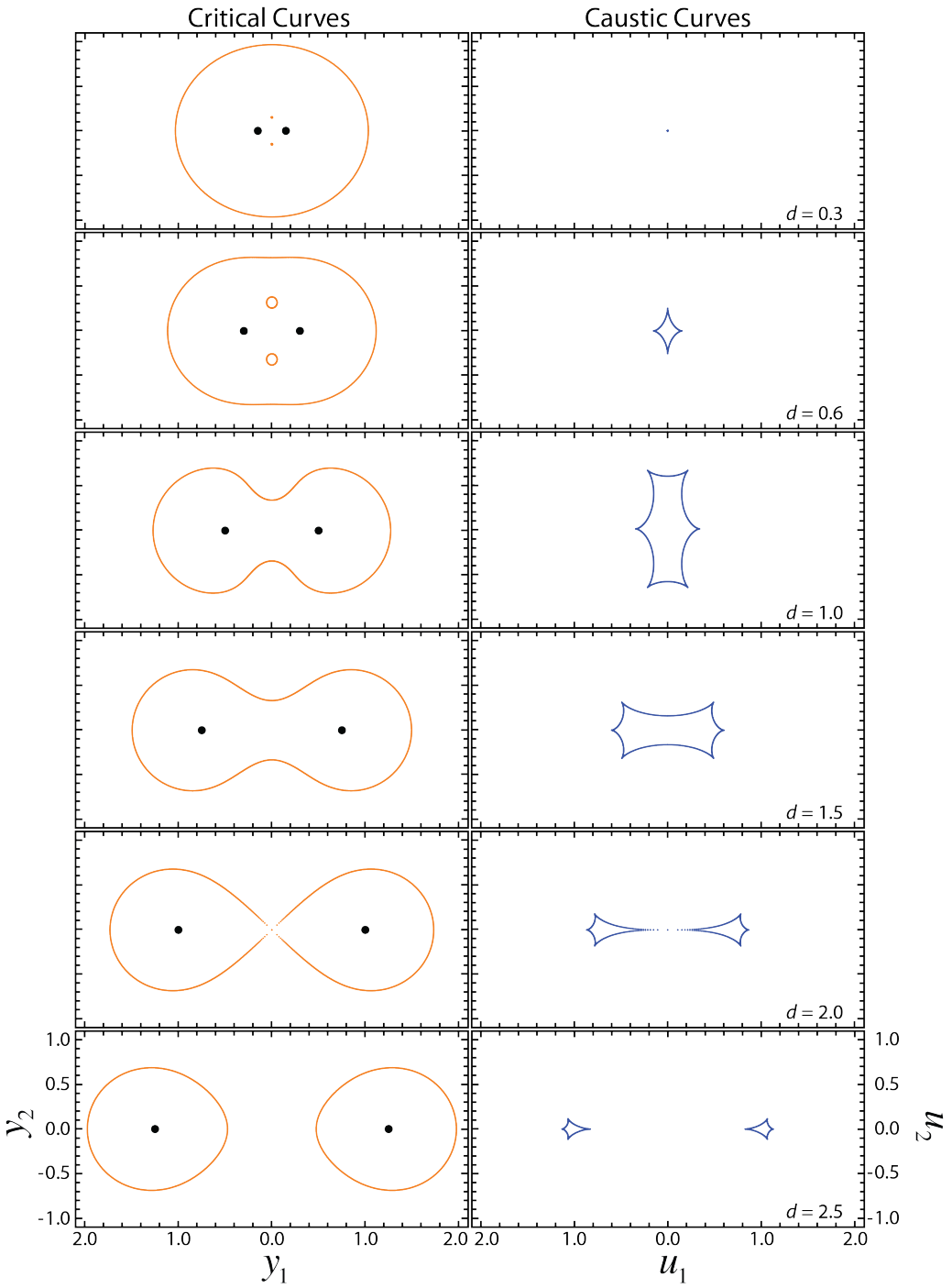

Figure 4.3: Critical and caustic curves for increasing values of the star-planet separation, d. The mass ratio is set to $q = 1$.

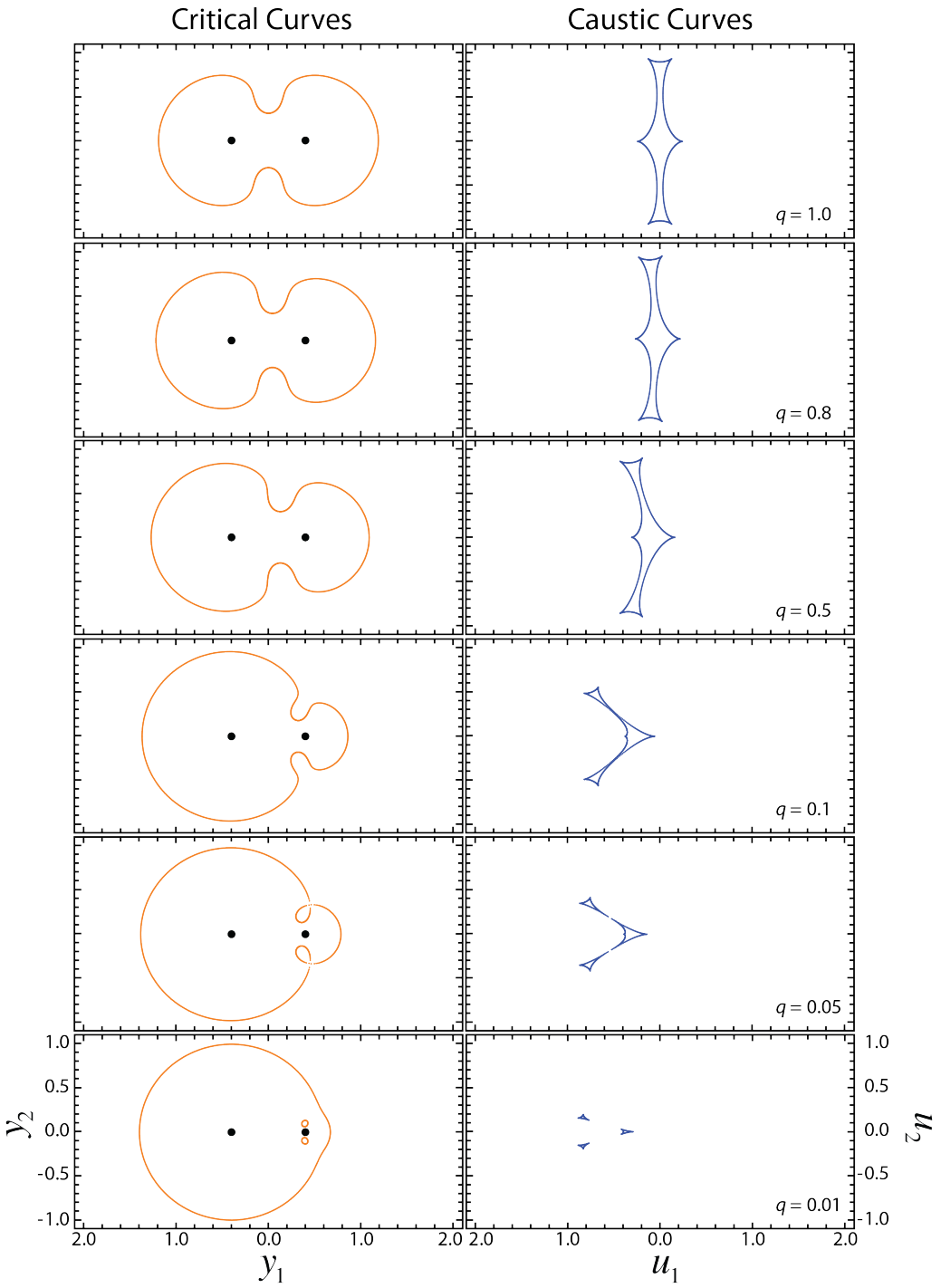

Figure 4.4: Critical and caustic curves for increasing values of the mass ration, q. The star-planet separation is set to $d = 0.8$.

4.5 Planetary Systems

For binary systems with the mass ratio $q \ll 1$ (corresponding to a planetary system), the intermediate regime is relatively small and contained to planet-star separations near $d = 1$. This is advantageous because the close and wide binary regimes will produce separate caustic curves associated with the parent star and the planet.[9] Below, we discuss the close and wide regimes in more detail and describe possible light curves that can result.

4.5.1 Central Caustics

For both the close and wide binary regimes, one caustic is always located near the position of the parent star. This caustic is known as the central caustic with a shape similar to that of an arrow which points toward the companion planet. The light curve of a source passing near the central caustic differs in shape depending on which part of the caustic the source passes near. A source passing near the back end of the central caustic perpendicular to the star-planet axis will exhibit a U-shape caused by the cups of the caustic (Figure 4.6b) , while a a source passing near the front tip of the caustic forms a single bump (Figure 4.6a). A source passing parallel to the star-planet axis near the central caustic will show little deviation from the single lens light curve, unless a caustic crossing takes place.[7] Figure 4.5 shows how the central caustic changes with d.

The central caustic is invariant under the transformation $d \rightarrow d^{-1}$, which means the central caustic formed in the wide regime ($d > d_w$) is indistinguishable from the central caustic formed in the close regime ($d^{-1} < d_c$).[7] For example, as shown in Figure 4.5, a central caustic formed for $d = 1.67$ is the same as the central caustic formed for $d = 0.6$. Thus, the light curves formed by a source passing near a central caustic is degenerate in d.

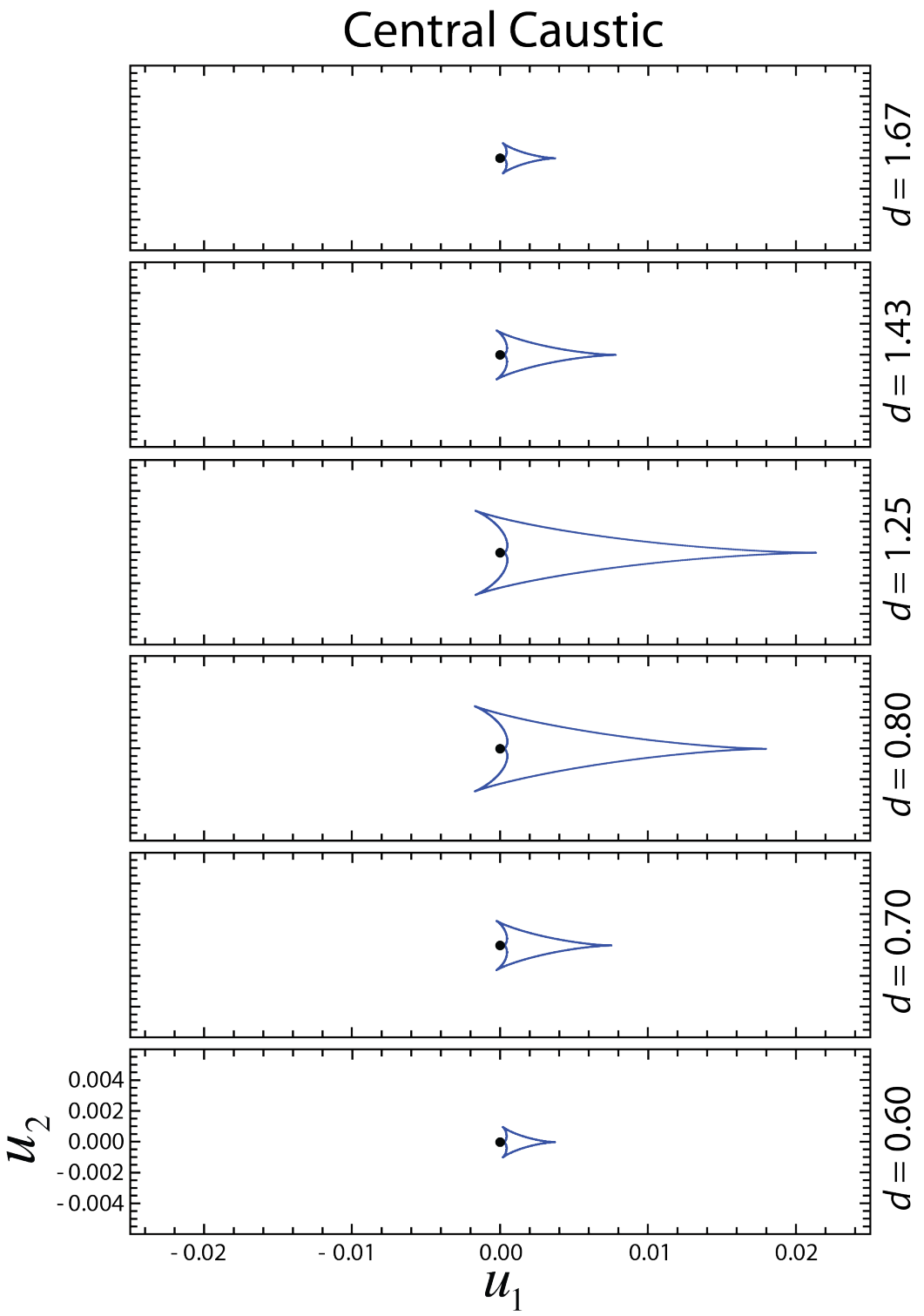

Figure 4.5: A central caustic shown for various values of d.

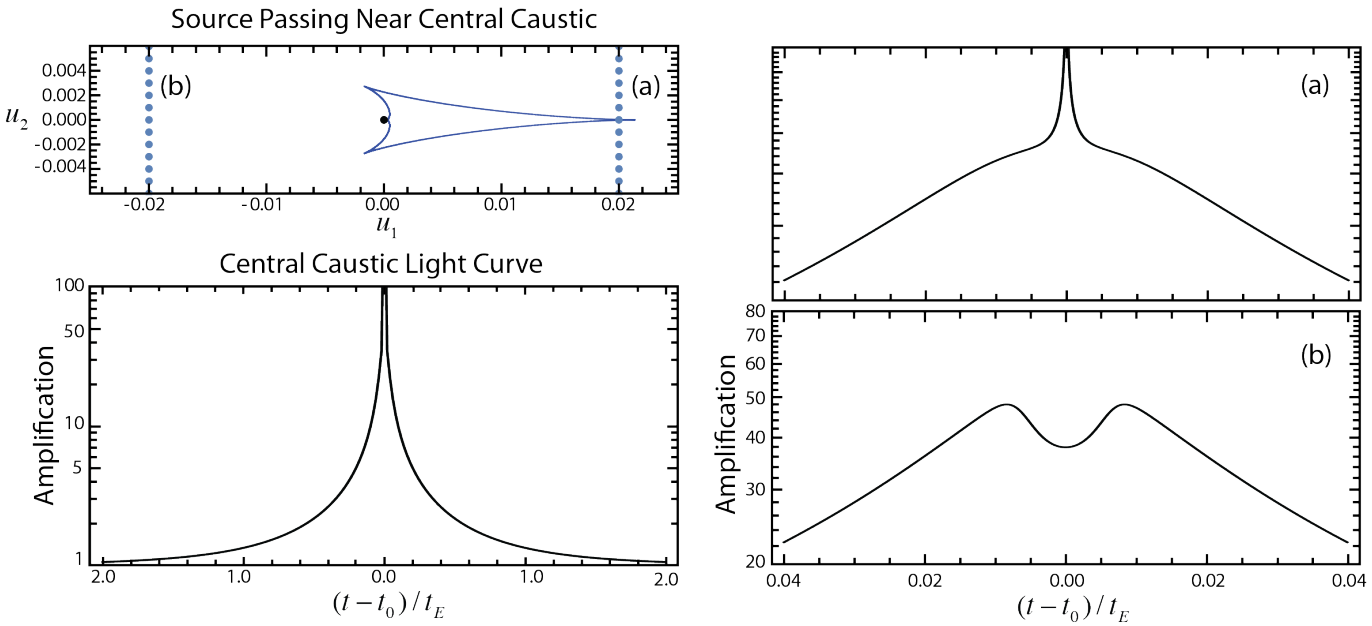

Figure 4.6: The top left plot shows a central caustic for $q = .001$ and $d = 1.25$. The blue dots show the trajectory of a source near the central caustic. The bottom left plot shows an overall light curve for both trajectories. Plot (a) shows a zoomed in light curve of the source trajectory (a) and Plot (b) shows a zoomed in light curve of the source trajectory (b).

4.5.2 Planetary Caustics

The close binary regime exhibits three caustics; the central caustic and two caustics known as planetary caustics. These planetary caustics have a triangular shape and form on the opposite side of the central caustic from the position of the planet.. They form symmetrically about the star-planet axis, with the distance between them increasing with decreasing d.[9] A source passing through the large region between the planetary caustics will form a light curve with a decrease in amplification (Figure 4.7b,c), while a source passing within a small region on the outside of the caustics will increase in magnification.[9]

The wide binary regime forms two caustics; the central caustic and one planetary caustic, shown in Figure 4.7d. The planetary caustic forms on the star-planet axis on the same side of the central caustic as the planet. The light curve exhibits bumps passing very near the cups of this caustic, and has little effect to the light curve if the source passes further away.

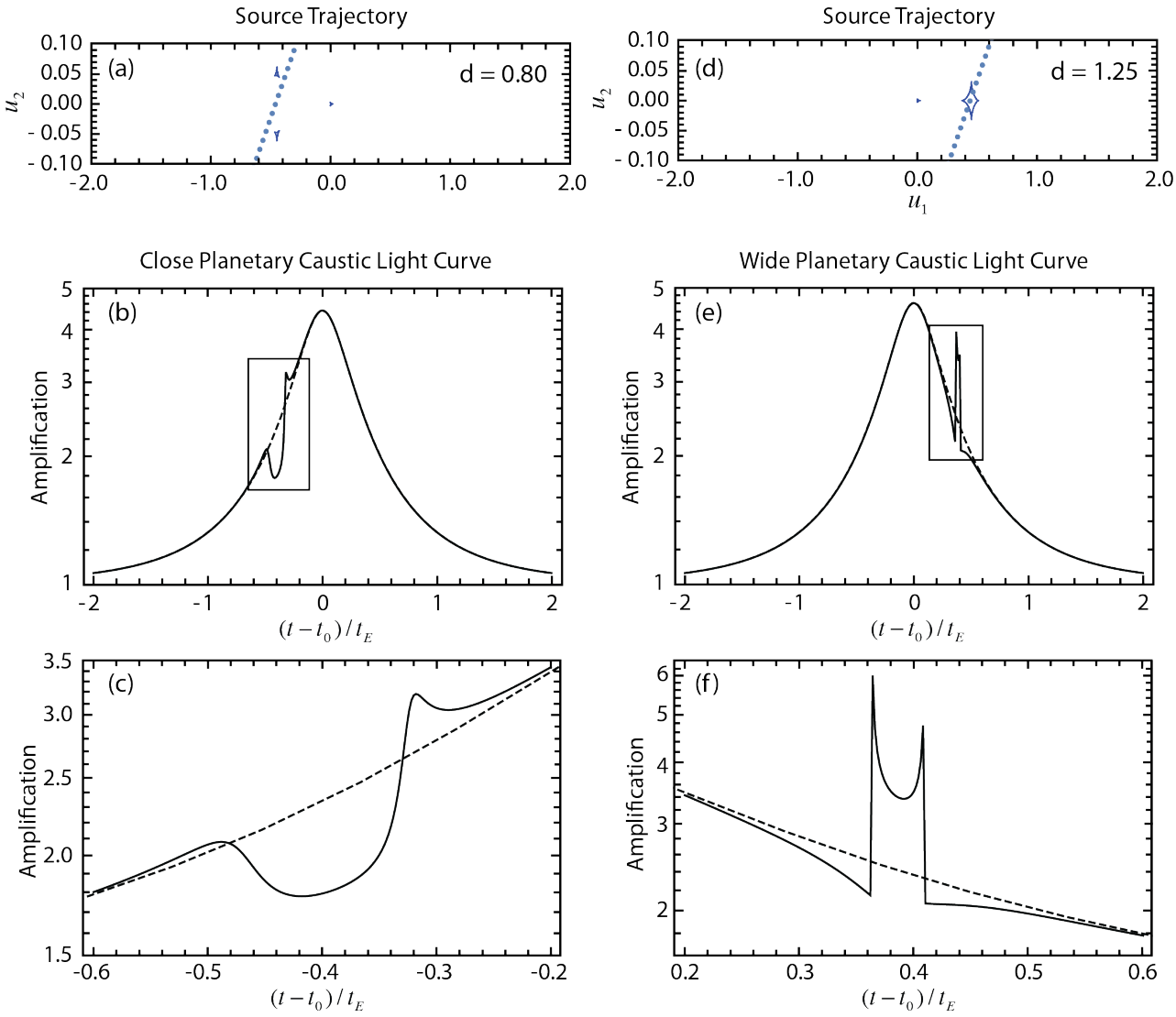

Figure 4.7: Plot (a) shows a close regime planetary caustic with $q = 0.001$ and $d = 0.8$. The blue dots show the trajectory of a source passing through the center of the planetary caustics. Plot (b) shows the resulting overall light curve and plot (c) shows a zoomed in region of the light curve. Plot (d) shows a wide regime planetary caustic where a source crosses the planetary caustic. The resulting light curve is shown in plot (e) and plot (f) is a zoomed in region of the light curve.

4.6 Binary Lens Images

The images formed by a binary system can be found by solving Equation 4.11. It is useful to rewrite Equation 4.11 as a 5th order polynomial in z. This is done by allowing the lenses to be placed along the real axis with $z_2 = -z_1$, and defining $m = (m_1 + m_2)/2$ and

$\Delta m = (m_2 - m_1)/2$. Taking the complex conjugate of Equation 4.11 and substituting the expression for $\bar{z}$ back into Equation 4.11 results in the polynomial of the form,[29]

$$p_5(z) = \sum_j^5 c_j z^j = 0 \tag{4.17}$$

where the coefficients c_j of the polynomial are given by,[29]

$$\begin{aligned}
c_5 &= z_1^2 - \bar{\zeta}^2 \\
c_4 &= -2m\bar{\zeta} + \zeta\bar{\zeta}^2 - 2\Delta m z_1 - \zeta z_1^2 \\
c_3 &= 4m\zeta\bar{\zeta} + 4\Delta m\bar{\zeta}z_1 + 2\bar{\zeta}^2 z_1^2 - 2z_1^4 \\
c_2 &= 4m^2\zeta + 4m\Delta m z_1 - 4\Delta m\zeta\bar{\zeta}z_1 - 2\zeta\bar{\zeta}^2 z_1^2 + 4\Delta m z_1^3 + 2\zeta z_1^4 \\
c_1 &= -8m\Delta m\zeta z_1 - 4(\Delta m)^2 z_1^2 - 4m^2 z_1^2 - 4m\zeta\bar{\zeta}z_1^2 - 4\Delta m\bar{\zeta}z_1^3 - \bar{\zeta}^2 z_1^4 + z_1^6 \\
c_0 &= z_1^2[4(\Delta m)^2\zeta + 4m\Delta m z_1 + 4\Delta m\zeta\bar{\zeta}z_1 + 2m\bar{\zeta}z_1^2 + \zeta\bar{\zeta}^2 z_1^2 - 2\Delta m z_1^3 - \zeta z_1^4]
\end{aligned}$$

In general, this polynomial cannot be solved analytically so numerical techniques must be used to solve for the images. It is important to note that, while solving $p_5(z)$ produces up to five solutions, not all of these solutions actually solve the lens equation.[29] Depending on the position of the source, two of the solutions may not correspond to the source positions in the lens equation. Thus there are either three or five solutions. If the source is outside of a caustic, there will be three real solutions. If the source is inside of a caustic, then all five solutions are valid. This is depicted in Figure 4.8.

4.7 Planetary Caustic Crossings

When a source passes through a caustic region during a microlensing event, the light curve produced has a very characteristic shape due to the sudden change in the number of images produced by the lens. These events are called caustic crossings. As the source enters a

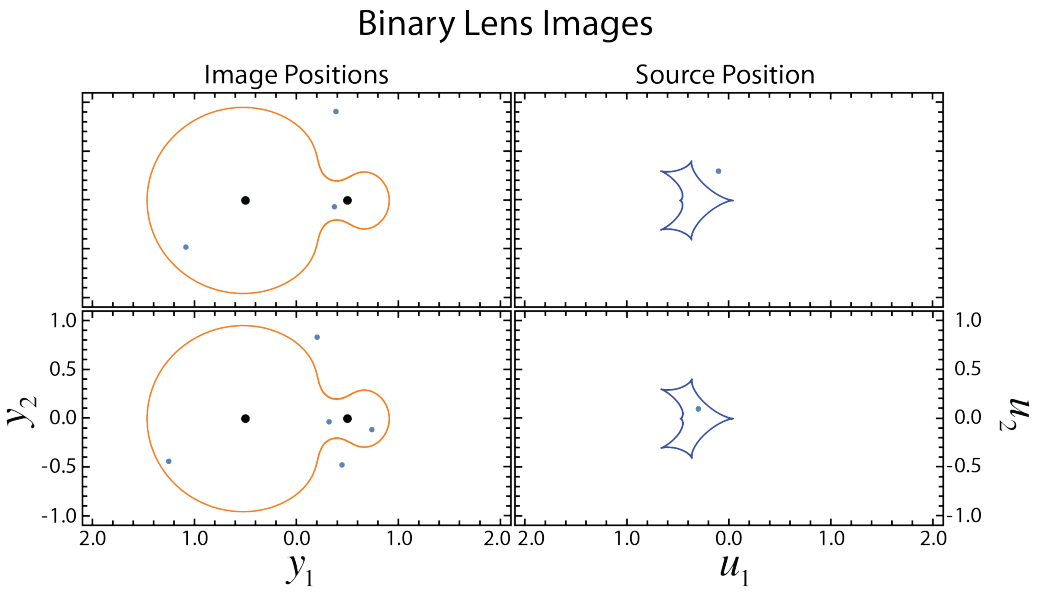

Figure 4.8: The position of the images for two source positions. When the source is outside of a caustic, 3 images are formed. When the source is within a caustic, five images are formed.

caustic region, the total number of images changes from three to five and the light curve exhibits a discontinuous increase in magnification, followed by a smooth decrease inside the caustic region. As the source exits the caustic region, the opposite behavior takes place with a smooth increase in magnification followed by a discontinuous decrease as the source crosses the caustic curve. The light curve then has two large peaks with a U-shape in between the peaks, as shown in Figure 4.7e,f. This is particularly advantageous for planetary caustic crossings. The light curve from planetary crossings allows one to determine the mass ratio of the lens and separation of the star and planet essentially by eye.

For planetary caustic crossings, it is useful to consider a complementary picture of what is occurring during these events.[10] Consider the path of the images produced by the lens system as a source moves across the sky. If a planet is located near the Einstein Ring of the parent star, as an image moves behind the planet, the planet acts as another lensing event resulting in a second amplification of the image.

We can treat the amplification due to the planet as analogous to the single lens amplification discussed above. We define the angular Einstein ring radius of the planet, $\theta_{E,p}$,

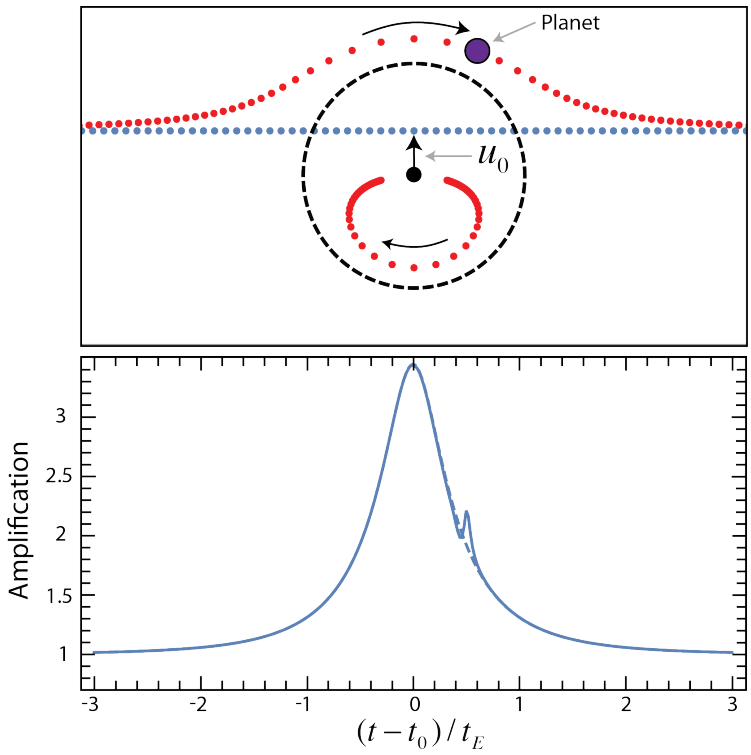

Figure 4.9: A diagram of how a planet can effect the image of a source during a microlensing event.

as,

$$\theta_{E,p} = \sqrt{\frac{(D_S - D_L)}{D_S D_L} \frac{4m_1 G}{c^2}} \tag{4.18}$$

and the Einstein crossing time of the planet, $t_{E,p}$, as,

$$t_{E,p} = \frac{\theta_{E,p}}{\mu_{rel}} \tag{4.19}$$

The parent star has its own angular Einstein ring radius and Einsein crossing time defined by,

$$\theta_E = \sqrt{\frac{(D_S - D_L)}{D_S D_L} \frac{4m_2 G}{c^2}} \tag{4.20}$$

$$t_E = \frac{\theta_E}{\mu_{rel}} \tag{4.21}$$

respectively. The ratio of the Einstein crossing times of the planet and its parent star give,[9][10]

$$\frac{t_{E,p}}{t_E} = \sqrt{\frac{m_1}{m_2}} = \sqrt{q} \tag{4.22}$$

t_E is found by the overall shape of the light curve, while $t_{E,p}$ is found by considering the planet amplification in isolation. In this way, the approximate mass ratio of the binary system is determined.

Because the image of the source passing the planet must be near the position of the planet in order to affect the overall light curve, we are able to determine the star-planet separation of the binary system from planetary caustic crossings as well. The separation, d, can be written as,[9][10]

$$d = y \pm u_p$$

where we define $u_p = \{u_0^2 + [(t_{0,p} - t_0)/t_e]^2\}^{1/2}$ to be the position of the source during the planetary perturbation, $t_{0,p}$. Note that there is a degeneracy in d. The third parameter that can be determined is the angle of the source trajectory relative to the star-planet axis, ϕ, by,[9][10]

$$\alpha = \sin\left(\frac{u_0}{u_p}\right)$$

The above equations are not exact, but serve useful for defining initial curve fitting parameters. The actual lensing parameters are found more accurately from the curve fitting routine.

For central caustic crossings, determining the lens parameters is not nearly as straight forward as for planetary caustic crossings. However, an understanding of the central caustic properties discussed above does enable one to guess initial fitting parameters.[9][10]

4.8 Determining Planet and Parent Star Masses

Detecting a planetary microlensing event requires the source to pass very near the caustics produced by a planetary system. This is essentially the same condition for finite source effects to become measurable. For most planetary microlensing events, we can deduce the angular Einstein radius of the system, θ_E, in much the same way that is done for single lens events. This was done by Bond et. al.[4] Figure 4.10 shows the observed light curve from the event. The event was a planetary caustic crossing. The mass ratio was found to be $q = .0039 \pm .0011$ while the star-planet separation was found to be $d = 1.12$. Using finite source effects, $\theta_E = 520 \pm 80\mu$as.

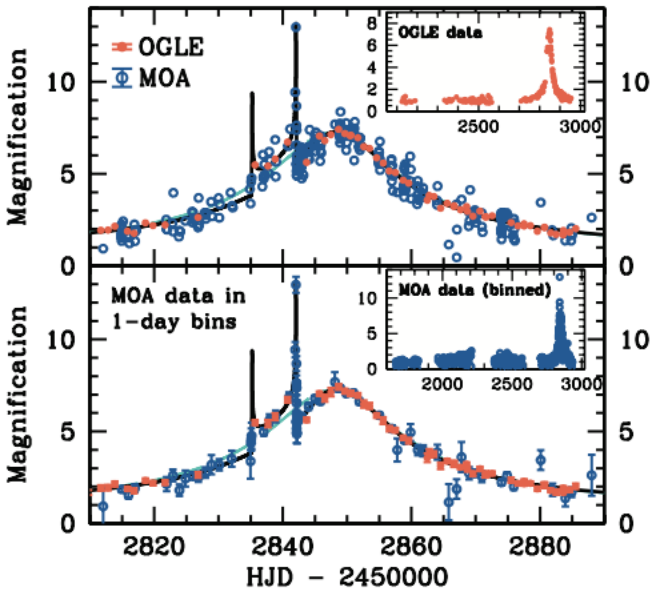

Figure 4.10: An observed binary microlensing event by Bond et. al.

Using satellites in conjunction with finite source effects allows for the determination of the mass of the planet in a binary system. This was done to analyze a light curve by Zhu.[34] The mass of the star and planet where found to be 0.94 ± 0.17 $M_\odot$ and 0.355 ± 0.079 $M_\odot$, respectively. Figure 4.11 shows a closeup of the caustic crossing from both Earth observatories and the Spitzer telescope.

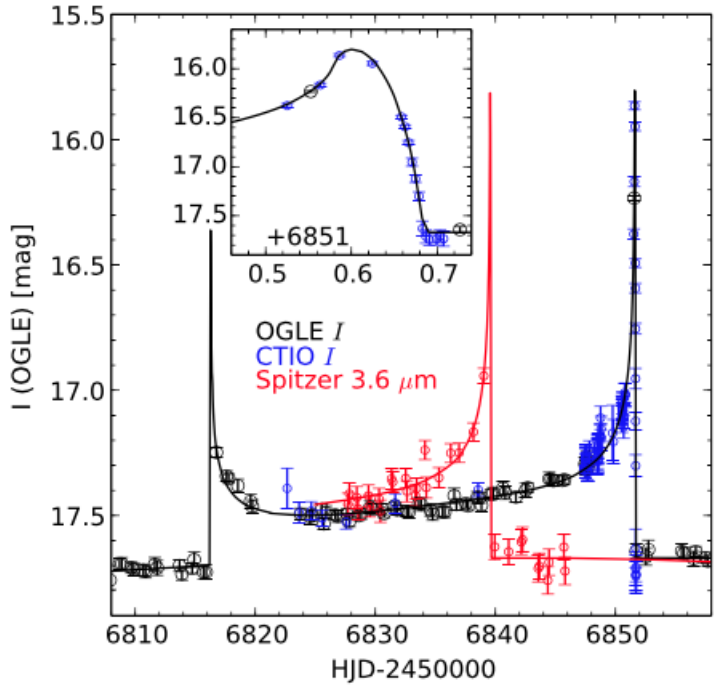

Figure 4.11: An observed binary microlensing event. The black curve is the best fit from data observed from earth while the red curve is the best fit from data observed from the Spizter telescope.

Bibliography

[1] C Alcock, WH Allen, RA Allsman, D Alves, TS Axelrod, TS Banks, SF Beaulieu, AC Becker, RH Becker, DP Bennett, et al. Macho alert 95-30: First real-time observation of extended source effects in gravitational microlensing. *The Astrophysical Journal*, 491(2):436, 1997.

[2] Ch Alcock, Carl W Akerlof, RA Allsman, TS Axelrod, DP Bennett, S Chan, KH Cook, KC Freeman, K Griest, SL Marshall, et al. Possible gravitational microlensing of a star in the large magellanic cloud. *arXiv preprint astro-ph/9309052*, 1993.

[3] Ch Alcock, RA Allsman, D Alves, TS Axelrod, DP Bennett, KH Cook, KC Freeman, K Griest, J Guern, MJ Lehner, et al. First observation of parallax in a gravitational microlensing event. *The Astrophysical Journal Letters*, 454(2):L125, 1995.

[4] Ian A Bond, A Udalski, M Jaroszyński, NJ Rattenbury, B Paczyński, I Soszyński, L Wyrzykowski, MK Szymański, M Kubiak, O Szewczyk, et al. Ogle 2003-blg-235/moa 2003-blg-53: a planetary microlensing event. *The Astrophysical Journal Letters*, 606(2):L155, 2004.

[5] Sean M Carroll. An introduction to general relativity. *Spacetime and Geometry. Addison Wesley*, 2004.

[6] J-Y Choi, I-G Shin, S-Y Park, C Han, A Gould, T Sumi, A Udalski, J-P Beaulieu, R Street, M Dominik, et al. Characterizing lenses and lensed stars of high-magnification

single-lens gravitational microlensing events with lenses passing over source stars. *The Astrophysical Journal*, 751(1):41, 2012.

[7] Sun-Ju Chung, Cheongho Han, Byeong-Gon Park, Doeon Kim, Sangjun Kang, Yoon-Hyun Ryu, Kang Min Kim, Young-Beom Jeon, Dong-Wook Lee, Kyongae Chang, et al. Properties of central caustics in planetary microlensing. *The Astrophysical Journal*, 630(1):535, 2005.

[8] Albert Einstein. Lens-like action of a star by the deviation of light in the gravitational field. *Science*, 84(2188):506–507, 1936.

[9] B Scott Gaudi. Exoplanetary microlensing. *arXiv preprint arXiv:1002.0332*, 2010.

[10] B Scott Gaudi. Microlensing surveys for exoplanets. *Annual Review of Astronomy and Astrophysics*, 50:411–453, 2012.

[11] A Gould, A Udalski, B Monard, K Horne, Subo Dong, N Miyake, K Sahu, DP Bennett, I Soszyński, MK Szymański, et al. The extreme microlensing event ogle-2007-blg-224: Terrestrial parallax observation of a thick-disk brown dwarf. *The Astrophysical journal letters*, 698(2):L147, 2009.

[12] Andrew Gould. Macho velocities from satellite-based parallaxes. *The Astrophysical Journal*, 421:L75–L78, 1994.

[13] Andrew Gould. Proper motions of machos. *The Astrophysical Journal*, 421:L71–L74, 1994.

[14] Andrew Gould. Microlensing and the stellar mass function. *Publications of the Astronomical Society of the Pacific*, 108(724):465, 1996.

[15] Andrew Gould. A natural formalism for microlensing. *The Astrophysical Journal*, 542(2):785, 2000.

[16] Andrew Gould and Abraham Loeb. Discovering planetary systems through gravitational microlenses. *The Astrophysical Journal*, 396:104–114, 1992.

[17] B Grieger, R Kayser, and S Refsdal. A parallax effect due to gravitational micro-lensing. *Nature*, 324(6093):126–127, 1986.

[18] Lindita Hamolli, Mimoza Hafizi, Francesco De Paolis, and Achille A Nucita. Estimating finite source effects in microlensing events due to free-floating planets with the euclid survey. *Advances in Astronomy*, 2015, 2015.

[19] Shude Mao. Introduction to gravitational microlensing. *arXiv preprint arXiv:0811.0441*, 2008.

[20] Shude Mao and Bohdan Paczynski. Gravitational microlensing by double stars and planetary systems. *The Astrophysical Journal*, 374:L37–L40, 1991.

[21] Silvia Mollerach and Esteban Roulet. *Gravitational lensing and microlensing*. World Scientific, 2002.

[22] Robert J Nemiroff and WAD Wickramasinghe. Finite source sizes and the information content of macho-type lens search light curves. *arXiv preprint astro-ph/9401005*, 1994.

[23] Bohdan Paczynski. Gravitational microlensing by the galactic halo. *The Astrophysical Journal*, 304:1–5, 1986.

[24] S. Refsdal and S. Rosseland. On the possibility of determining the distances and masses of stars from the gravitational lens effect. *Monthly Notices of the Royal Astronomical Society*, 134(3):315, 1966.

[25] Sjur Refsdal and H. Bondi. The gravitational lens effect. *Monthly Notices of the Royal Astronomical Society*, 128(4):295–306, 1964.

[26] P Schneider. E hlers j. & falco ee, 1992,g ravitationallenses.

[27] Peter Schneider and Achim Weiss. The two-point-mass lens-detailed investigation of a special asymmetric gravitational lens. *Astronomy and Astrophysics*, 164:237–259, 1986.

[28] Hans J Witt and Shude Mao. Can lensed stars be regarded as pointlike for microlensing by machos? *The Astrophysical Journal*, 430:505–510, 1994.

[29] Hans J Witt and Shude Mao. On the minimum magnification between caustic crossings for microlensing by binary and multiple stars. *The Astrophysical Journal Letters*, 447(2):L105, 1995.

[30] HJ Witt. Investigation of high amplification events in light curves of gravitationally lensed quasars. *Astronomy and Astrophysics*, 236:311–322, 1990.

[31] JC Yee, A Udalski, S Calchi Novati, A Gould, S Carey, R Poleski, BS Gaudi, RW Pogge, J Skowron, S Kozłowski, et al. First space-based microlens parallax measurement of an isolated star: Spitzer observations of ogle-2014-blg-0939. *The Astrophysical Journal*, 802(2):76, 2015.

[32] Jaiyul Yoo, DL DePoy, A Gal-Yam, BS Gaudi, A Gould, C Han, Y Lipkin, D Maoz, EO Ofek, B-G Park, et al. Ogle-2003-blg-262: finite-source effects from a point-mass lens. *The Astrophysical Journal*, 603(1):139, 2004.

[33] Wei Zhu, S Calchi Novati, A Gould, A Udalski, C Han, Y Shvartzvald, C Ranc, UG Jørgensen, R Poleski, V Bozza, et al. Mass measurements of isolated objects from space-based microlensing. *The Astrophysical Journal*, 825(1):60, 2016.

[34] Wei Zhu, A Udalski, A Gould, M Dominik, V Bozza, C Han, JC Yee, S Calchi Novati, CA Beichman, S Carey, et al. Spitzer as a microlens parallax satellite: Mass and distance measurements of binary lens system ogle-2014-blg-1050l. *The Astrophysical Journal*, 805(1):8, 2015.